CHARACTERISTICS OF HYDROGEN FUEL COMBUSTION IN A REHEATING FURNACE

by

Chukwunedum Uzor

A Thesis

Submitted to the Faculty of Purdue University

In Partial Fulfillment of the Requirements for the degree of

Master of Science in Mechanical Engineering

Department of Mechanical and Civil Engineering

Hammond, Indiana

December 2022

THE PURDUE UNIVERSITY GRADUATE SCHOOL
STATEMENT OF COMMITTEE APPROVAL

Dr. Chenn Q. Zhou, Chair

Department of Mechanical and Civil Engineering

Dr. Nesrin Ozalp

Department of Mechanical and Civil Engineering

Dr. Xiuling Wang

Department of Mechanical and Civil Engineering

Approved by:

Dr. Chenn Q. Zhou

This work is dedicated to Yeshua, my wife, parents, siblings and best friend who despite the challenges of life, always support me in all that I do.

ACKNOWLEDGMENTS

My utmost acknowledgement goes to God Almighty, who never turns back on me. You knew me from my mother's womb and has the blueprint of my life and being. Yeshua, you paved the way for me through both lack and abundance, you gave me health and hope even when I couldn't see the light at the end of the tunnel. The underserved divine wisdom, understanding, and knowledge you graced me with is astonishing and dumfounding. Thank You!!!

My sincere gratitude goes to the Steel Manufacturing Simulation and Visualization Consortium for pioneering and fully supporting the hydrogen project for the steel industry. I also want to thank the Project Technical Committee Members (PTC) for both the reheat furnace section and all other sections of SMSVC for their numerous input and guidance in the unexpected progress of this work. Special thanks to Center for Innovation through Visualization and Simulation for grooming all the talents I had in me. CIVS laid out an astute platform and personnel development program for student research nurturing of which I was a core benefit of. They shaped my research abilities, presentation, time management, work place relationship skills and all other ramifications of my life. It was really exciting, refreshing and life reforming to have once been a part of system.

I will like to acknowledge my academic advisor, Professor Chenn Q. Zhou, for offering me a rare opportunity to be part of improving the steel industry as they evolve. Her advices, push and encouragement makes her one of a kind, I wouldn't have been a better research student under any other tutelage. I will also want to use this space to thank Professor Xiuling Wang, Professor Nesrin Ozalp, Professor Nicholai Tafulae and Professor Armin Silaen for passing across a wealth of analytical and engineering knowledge in and out of the classroom. They were also responsible for making sure my thesis work was flawless and of the required standard of which they did an outstanding review that was part of my amazing success.

Professor Armin Silaen, Professor Tyamo Okosun, Dr. Orlando Ugarte, and Nick Walla, have also been very instrumental to my growth. I simply couldn't have finished my consortium projects successfully without their patient and kind continual guidance. They carried me as a brother, friend and student and were so close to the level where I shared private matters and got

personal advices that motivated me to keep going. They instilled in me an analytical and stepwise problem solving culture that has distinguished me as an excellent engineer. I can't ignore the input of my former and present colleagues, John Rosser, Emily Higley, Anurag Karambelkar, and Imran Syed for always being diligent in working as a team, surmounting unimaginable feats and made me feel like a great leader. To Rashed El-Manasir, Neel Busa, Xipeng Guo, Sam Wilson, Akshita Mogali, Saswot Thapa, Pavan Vamula, Yanan Song, Mingqian Wang and Ninad Patil I say a huge thank you for all the tutorials and fun times. I will never forget all of you in a hurry.

I will also like to thank my best friend Williams Oged and his wife Ogochukwu Duruiheme for being there for me through thick and thin. Their warm encouragements, physical gifts and immense love they have for me has been unmatched. I love you all so much and I promise to always be there for your family anytime and always.

Lastly, I want to thank my beloved wife who has been with me through it all. The love she has for me has kept me going through the rigors of research. Her daily encouragement and prayers has been the fuel that keeps me going. For all you do, thank you Sweetheart. I can't forget my parents; Mr. and Mrs. Michael Uzor for their parental and spiritual support through the journey of life. You two have been there for me through sickness and health, and I wouldn't have gone this far if not for your advices and grooming. Thanks to Onyinyechukwu Eze and Chukwuemeka Uzor, my two beloved siblings who are dear to my heart. Thank you so much.

TABLE OF CONTENTS

LIST OF TABLES

LIST OF FIGURES

ABSTRACT

Current industrial practice in the steel Industry involves the use of natural gas with high methane content as a primary energy source. Natural combustion produces greenhouse gases, and with the continued focus on managing and reducing harmful emissions from industrial processes, there is a need for research into alternative sources of energy. Among several alternatives that have been studied is hydrogen: a non-carbon-based fuel. This work uses a coupled computational fluid dynamics (CFD)-finite element analysis (FEA) combustion model to investigate hydrogen utilization as a fuel in a reheat furnace and how it impacts the quality of the steel produced by understanding the three dimensional (3D) flow behavior, furnace temperature profile, thermal stress distribution, heat flux, formation of iron oxides, emission gases and mode of heat transfer onto the steel slabs. The modeling process integrates the five different zones of a pusher type reheating furnace (top and bottom) and modeled using Ansys Fluent 2020R1 and Ansys Workbench 2022R1. Changes in these parameters are determined by comparison to a baseline case that uses methane as fuel and maintaining the same heat input in terms of chemical energy into the furnace. Global mechanism was used for hydrogen and two step mechanism was used for methane combustion. Results revealed a 2.6% increase in average temperature to 1478K across the furnace for hydrogen which resulted in 6.45% increase in maximum heat flux into the slabs. Similar flue gas flow patterns were seen for both cases and heat transfer mode from the combustion gases to the slabs was primarily by radiation (~97%) for both methane and hydrogen. 11.5% increase in iron oxide formation on the slab was recorded for the hydrogen case, however, the bulk of the iron oxide formed was more of wüstites which are the easiest form of iron oxide to descale. However, elevated nitrogen oxide (NOx) levels were recorded for hydrogen combustion which led to further study into NOx mitigation techniques. Application of the staged combustion method using hydrogen fuel showed potentials for NOx reduction. The use of regenerative burners further conserved exergy losses in hydrogen fuel application. Insignificant deviation from base case thermal stress distribution and zero carbon emission from the hydrogen case indicates the usability of hydrogen as an alternative fuel in reheating furnace operations.

1. INTRODUCTION

1.1 Reheat furnace overview

Steelmaking Industry produced in 2018 around $137 billion [1]. Economical operations and high-quality products are important goals for all steelmakers, and efforts to improve product quality and reduce costs are always ongoing. Iron and steel production can roughly be divided into four stages: ironmaking, steelmaking, hot rolling, and cold rolling.

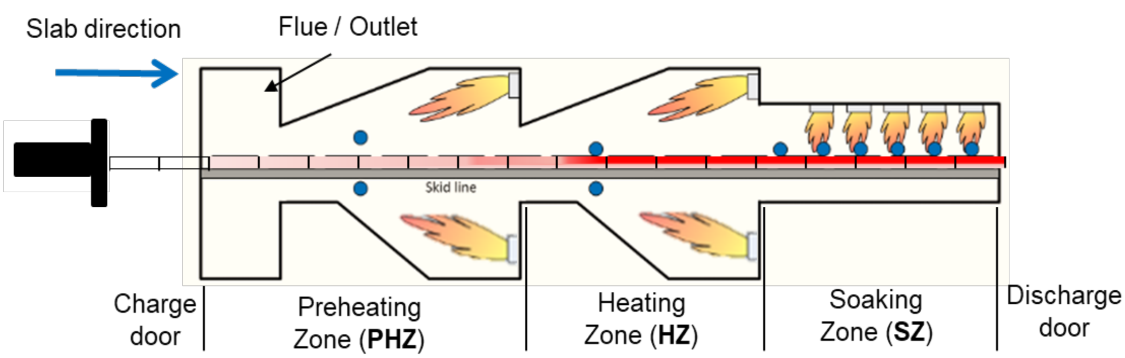

Figure 1. Reheating Furnace Process.

One of the most essential operations in steelmaking that affects product quality is the reheat furnace. Reheat furnaces which is also the second most energy consuming in steelmaking, are used in hot strip mills to reheat slabs to a uniform temperature before the hot rolling process [2]. In a reheating furnace, the steel slabs are heated to about 1500K or any required temperature as the temperature may vary by steel grades and can withstand up to 2 hours of exposure in the furnace [3]. Typical reheat furnaces as shown in Figure 1 are made up of three zones; preheat zone, heat zone and soak zone and they play separate roles in proper heating and temperature distribution into the slabs. In the preheat zone, the slab is gradually heated with low temperature gradient to prevent deformations and heated up properly to the desired temperature in the heating zone before it enters the soak zone where the temperature is evenly distributed through the entire slab. Convection and radiation are the primary methods for transferring heat from combustion gases to steel slabs in a reheat furnace [4].

1.2 Motivations and objectives

The application of hydrogen as a fuel has become a topic of high interest in the past decade by researchers in various industrial sectors. This stems from a global movement on curbing practices that generate greenhouse gases as they contribute largely to global warming. Among the greenhouse gases that contribute to global warming, carbon dioxide (CO_2) is a major player. This has resulted in global political sanctions to further reduce CO_2 emission. Several human activities have been found to release CO_2 into the atmosphere. Activities like transportation, manufacturing, lumbering, abrupt increase in farming areas and modern development are all culprits. According to the United States Environmental and Protection Agency, the steel industry contributes about 9% of the global CO_2 emissions. This gravely emphasizes the importance of regulating CO_2 emission in the steel industry. The reheating furnace is one of the most energy intensive equipment in the steel mill and emits a good amount of CO_2 since most steel companies use natural gas as fuel to combust its burners in other to effectively heat up the steel to a desirable temperature. This is why a non-carbon-based fuel like hydrogen has been considered as a fuel for the process of reheating slabs.

The transition from natural gas to hydrogen in the reheating furnace has raised the following questions:

- Will there be a need for burner redesign?
- Can hydrogen effectively heat up the slabs
- Will there be a change in product quality with hydrogen fuel?
- Will hydrogen fuel mitigate the emission of other pollutant gases like NOx?

This study is focused on answering these questions troubling the steel manufacturers. Hence, the objective of this study is to evaluate the potential use of hydrogen as a fuel in the reheating furnace, using the same burner configuration as with methane. As well as tracking several parameters that can affect product quality such as furnace temperature distribution, heat flux into the material, energy efficiency, scale formation on steel slabs, NOx formation, and thermal stress of the material. Studying these parameters will give an insight into hydrogen application in the reheat furnace and also help develop techniques for process optimization with hydrogen fuel.

1.3 Simulation software

Computational fluid dynamics (CFD) and other numerical analysis methods and algorithms are utilized to adequately study and analyze complex fluid movements within any environment. This covers many facets of thermodynamics, heat transfer in combustion systems and very complicated chemical reactions. For more than three decades now, its application has become increasingly popular as it saves time, cost and prevents hazards. It makes carrying out dangerous experiments under very hazardous conditions possible. Computational models primarily make use of three governing equations namely: mass, momentum and energy conservation equations. Developing in-house codes for a combustion model will be great however, due to time savings ANSYS commercial simulation software and MATLAB was used for this study. The combustion model was developed using ANSYS FLUENT, the thermal stress study was done using ANSYS WORKBENCH and scale thickness model was developed using and integration of MATLAB and Excel.

2. LITERATURE REVIEW

2.1 Combustion in reheating furnace

The achievement of both temperature increment, temperature uniformity and increased productivity requires a considerable amount of energy which has raised concerns towards energy and exergy efficiency optimization in the steel industry [5]. Also, with the increased dependency on steel for modern infrastructure, there have been rising environmental sustainability distresses due to the carbon emission composition of flue gases from the reheating furnace [6]. In the last two decades there has been a sharp increase in carbon emissions which has been linked to modernization as it led to increased utilization of carbon-based fuels [7]. Globally, water body temperatures have been seen to have increased by about 3K which is detrimental to our environment [8]. These recent uncomely environmental scares contributed by industrial emissions have triggered stringent emission regulations on manufacturing industries around the world. This has resulted in a shift from natural gas which has been the primary energy source used by most industries to alternative energy sources that can minimize or further eliminate greenhouse gas generation. Various alternatives have been postulated for the reheat furnace such as induction heating, direct electrification, biofuels, hydrogen injection, oxygen enrichment, full hydrogen utilization [9] etc. According to studies by Bloom Engineering, modern de-carbonization will involve the above mentioned in different magnitudes [9].

In another study by Bloom Engineering, they pointed out that although the combustion of hydrogen is carbon-less, parametric studies must be done to ascertain its viability, cost effectiveness and safety [10]. These reinforce the dire importance of the research into the use of hydrogen as a primary energy source in the reheat furnace.

Research on the use of natural gas revealed low flame speed that delineates burner operation and can result in generation of unburned carbon [11]. Hydrogen has been seen to possess faster flame speed that promotes flame stability and allows its operation to equivalence ratios of 0.5 [12]. Since hydrogen is not a carbon-based fuel, its flue gas components will be void of traces of carbon, making it a good fit and an alternative energy source as the world moves toward carbonless energy sources [13]. However, the switch from natural gas to hydrogen or any other fuel type will not thrive successfully if it has detrimental effect on the product quality. Certain combustion characteristics are paramount to achieving high quality product. In this study we will be using a computational fluid dynamics (CFD) platform to carry out a comparative investigation focusing on flow of combustion gases, furnace average temperature and heat transfer analysis of hydrogen against natural gas as factors to watch in order to maintain adequate and standard slab reheating operations.

In a reheating furnace, the major heat transfer mode is by the radiation from both combustion gases and furnace walls which makes up to 90% of the heat conveyed onto the slab [14]. Heat transfer through convection and conduction within the slab also takes place but not as conspicuous as thermal radiation [15]. Numerous mathematical models have been formulated over the decades to represent the complex heat transfer physics that occur in a regular reheating furnace and used to make several mathematical based software [16]. Earlier, these models only calculated conduction within slabs by making several assumptions on gas temperatures and heating coefficients gotten experimentally from furnaces and that simplified the formulas [17]. Subsequently, models were developed to mathematically represent thermal radiation using the zone technique which put into consideration the number of zones in the furnace [18]. Because these models neglected the effects of flow fields in the furnace atmosphere, they proved to be inaccurate [19]. Studies continued and CFD models that were accurate in predicting thermal radiation, furnace temperature and flow field were developed, however, it involved series of governing equations that made these models very computationally expensive and somewhat difficult to execute [20]. In the works of Han et. al. innovative mathematical methods that accounted for the transient thermal radiation onto the slabs and walls of the reheat furnace were put in place [2]. In the works of Han et al., a User Defined Function (UDF) was developed using the C computer language, to account for slab movement as Fluent software at that time didn’t have inbuilt functions capable of simulating slab movement. With 55 slabs moving through the furnace and convergence achieved, Han et al. was able to study the effect of skids on thermal radiation into the slab during the reheating process, and it was concluded that the presence of skids limits the radiative heat transfer in the lower half of the reheating furnace.

As the research into the heat transfer models evolved, relevant contributions were made by various researchers that were both computationally effective and accurate. Markov and Krivandin successfully carried out extensive research modelling of the steady state radiative heat transfer characteristics in walking beam and pusher type reheating furnaces using experimental results for continuous flow of gases and steel slabs in the furnace and showed that heat transfer in the reheat furnace was by radiation [21]. Further computational investigations on the effect of change in convective heat coefficient on the flow and temperature behavior was successfully carried out [22]. Results from the research showed that convective heat transfer is negligible and change in the convective heat transfer coefficient had little or no effect on the furnace atmosphere. Tang et al. [23] used Fluent code to model the pusher type furnace where fluid dynamics, radiation and combustion where not neglected and saw that there was a vortex under the slabs and bottom heating burners that resulted in a reverse flow in the lower portion of the furnace. Kim developed a mathematical model for predicting heat flux distribution in a slab for a walking beam reheat furnace which has been replicated by other researchers to give acceptable results [24]. In another work, Han et al. utilized the weighted sum of grey gases model (WSGGM) in predicting accurately radiation in a walking beam furnace [2]. Singh and Talukdar in recent research on a walking beam furnace determined that the most dominant heat transfer mode in the reheat furnace is the radiative heat transfer [25].

Study on the use of hydrogen in an entire reheat furnace and its combustion characteristics is scarce; a situation this study intends to address. In this work, CFD is used to model radiation, combustion and fluid flow of natural gas and hydrogen in a 3D reheat furnace domain. The furnace type is a walking beam reheating furnace modelled for steady state radiation, temperature distribution and fluid flow. The radiation model used was the discrete ordinate in FLUENT [26]. This study uses natural gas as baseline to compare parametric values against hydrogen utilization. This present method is very flexible as it can incorporate transient studies and complex geometric modification into its analysis with little adjustments. This research aims to answer the questions pertaining to heat transfer mode and fluid flow changes with hydrogen fuel. Results shown will also give industry insight into the impact of using hydrogen as fuel in the reheat furnace.

2.2 Thermal stress in reheating furnace

During the steel making process steel that has been produced is mechanically deformed, via the rolling process, to the desired size of the final steel product. The steel is first heated to increase its ductility so that the rolling process is economically feasible and so that the final steel product has the proper microstructure and properties [27,28]. The heating of steel takes place by moving the steel through a large multi-zone industrial combustion furnace called a reheat furnace. Reheat furnaces are divided into multiple zones that allow for controlling the rate of heat supplied to the steel. This is to ensure that the steel is not too rapidly heated which can damage the product via large thermal stresses [29]. Because of the amount of heat that needs to be supplied to the steel, the reheating process is the second most energy intensive step of the steel making process [32].

There is a high demand for quality steel and given the reheat process' importance in obtaining the final steel product properties and its high energy demand there is much interest in studying the process [30]. Reheat furnace studies often focus on how to improve furnace efficiency, reduce environmental impact, reduce scale formation, and to determine hard to measure parameters such as thermal stresses. Numerical models using computational fluid dynamics (CFD) and finite element analysis (FEA) techniques have proven useful in predicting and developing understanding of heat transfer characteristics, scale formation, and chemical kinetics [26,31]. These models provide insights into furnace operation that would otherwise be hard to measure.

When the steel enters the furnace in the form of slabs, billets, or bloom they are exposed to a heat flux primarily due to radiative heat transfer from methane combustion. The steel is transiently heated to the desired temperature creating temperature gradient thorough the steel [3,32]. The increase in temperature causes the steel to expand and thermal stresses are present due to the temperature gradients. Thermal stresses higher than the normal operating conditions, can damage the steel creating cracks and defects that carry over into the final product. Determining the thermal stress within the steel during normal operation of the reheat process is not feasible. Numerical modeling of the reheat process is useful to determine the expected thermal stress values.

This paper uses a validated CFD, and FEA coupled model to predict the thermal stress within steel slabs as they move through a pusher type reheat furnace, during baseline operation. The model is then used to predict the thermal stress when hydrogen combustion, using the same energy input, is used instead. The baseline thermal stress results using methane combustion and the H_2 thermal stress results are compared to determine if H_2 is a suitable substitute with respect to the impact on thermal stress.

2.3 Scale formation in reheating furnace

A major steel slab heating challenge in the reheat furnace is the formation of iron oxide that can also commonly known as scales. The process of scale development is highly complicated and is reliant on a wide range of factors. The slab spends about two hours in the furnace from start to finish and is heated to temperatures above 1500K. Primary scale is a layer of iron oxide scale that develops on the slab's outside due to the circumstances within the furnace. Before the slab can be processed further, this primary scale must be removed, which has been shown to result in a loss of 1-2% of the overall steel yield [3,33]. Since the scale layer's iron oxides all have poorer thermal conductivities than steel, less heat is transferred to the slab, which results in the manufacturing of lower-quality steel. Scaling can also limit the life of the hot rollers by causing damage to them during future processing. In order to attempt to estimate and anticipate the creation of scale inside the reheating furnace and reduce the weight lost due to oxidation, a fundamental understanding of oxidation and the kinetics of scale growth is required. The scientific community now has a better knowledge of oxidation thanks to the numerous experimental research on scale formation. However, the majority of these studies do not take into account how this knowledge might be applied and instead concentrate only on the kinetics of scale building.

Less research has been done on the impact of scale on heat transport inside non-isothermal, quaternary environments like reheating furnaces. In order to imitate the production of scale and attempt to collect important and accurate data, experimentation is typically carried out using a thermo-gravimetric analysis or a small furnace [34]. Depending on how the experiment is set up, these trials may be expensive to conduct and produce erroneous results. Scale adhesion problems and over-temperature are two well-known challenges with scale creation experiments. The consequences of various variables on scale development and the effects that scale has on slab reheating can be more accurately predicted using numerical approaches like computational fluid dynamics (CFD), which are less expensive.

The kinetics of scale growth has been the subject of numerous investigations as well as scale properties. Above 872K, Padassi discovered that iron oxide scale forms a three-layered structure. with a wüstite : magnetite : hematite composition ratio of 95:4:1 [35]. According to Akiyama et al., the thermal conductivities of all forms of iron oxide found on the scale are much lower than those of steel and follow a linear function of temperature [36]. The oxidation process begins with a linear trend and progresses over time to a parabolic trend. Smeltzer, discovered that the linear oxidation rate is much more sensitive to the atmosphere than to the gas temperature, implying that it is controlled by gas phase mass transport.[37] Additionally, Sachs and Tuck found that the temperature is the only factor that affects the parabolic regime, which is independent of gas composition [38]. The parabolic regime is controlled by the solid-state diffusion of iron ions via the scale layer. According to Selenz, Oeters, and Abuluwefa et al. [39,40], CO_2, H_2O, and O_2 all contribute equally to the linear rate of oxidation.

It has been convincingly shown that the linear and parabolic laws are appropriate for characterizing the oxidation process, including the impacts of CO_2 and H_2O, based on all of the investigations on the oxidation process stated above. To ascertain the linear and parabolic response rate constants of various steel grades, numerous researchers started working on studies in the late twentieth century as a result. Low-carbon steel oxidation rate constants were calculated using isothermal tests by Abuluwefa et al. at temperatures between 1273K and 1523K [41]. The oxidation process, including the impacts of CO_2 and H_2O, is adequately described by the linear and parabolic laws, as shown by all of the studies on the subject that have been discussed above.

The rapid advancement of methodologies utilizing computational fluid dynamics (CFD) in recent years has led to the widespread usage of computational simulation as a way to investigate fluid flow and heat transfer issues. In order to thoroughly examine furnace behavior, recent work has made substantial progress in simulating the three-dimensional reheating furnace. In a reheating furnace with a walking hearth design, Prieler et al. predicted the heating characteristics of billets using CFD approaches. For studying the transient heating process, CFD methodologies linking combustion reactions with the heating process were shown to be time-effective. [42]. A novel solution strategy was tried utilizing CFD modeling techniques to take the transient heating process in a three-dimensional walking hearth furnace into consideration, and it turned out to be a practical substitute.

Studies on alternative fuel utilization will not be wholesome without investigating the scale growth rate associated with the alternative fuel of interest. Recent studies have shown the use of hydrogen fuel increases scale formation by a range of 7% to 14%. However, studies have shown that descaling the scale formed by hydrogen will not be more difficult than that from natural gas combustion. This could be attributed to the low oxygen concentration across the furnace while burning hydrogen fuel which is needed for the formation of higher oxide scales which are more difficult to descale. Vladmir et. al. reported in his work that though the thickness of the scale increased with products of hydrogen combustion, the higher percentage of the scale where wüstites which are easy to descale. As part of the study on the characteristics of hydrogen fuel combustion in a reheating furnace, a scale predictor was developed based on the validated kinetics from the works of Abuluwefa using an integration of CFD and MATLAB codes.

3. METHODOLOGY

3.1 Numerical models

For this steady state study, the reheat furnace simulation was governed by integrating the Navier-Stokes and energy equations over the furnace domain. The species transport model was used to track combustion species concentration and distribution in the furnace. Couple solver was activated with k-epsilon turbulent model since the reaction was a turbulent reaction. For accuracy of the chemical reactions, the integrated finite-rate/Eddy dissipation model was applied. The governing equations used for the baseline case was retained for the hydrogen case as well.

3.1.1 Governing equations

Mass conservation equation

$$\frac{\partial \rho}{\partial t} + \nabla.(\rho u_i) \tag{1}$$

Momentum and conservation equation

$$\frac{\partial}{\partial x}(\rho u_i) + \nabla.\left(\rho u_i u_j\right) = -\nabla_p + \nabla.(\tau) + \rho g_i + F \tag{2}$$

In the above equation, ρ represents static pressure, ρg_i and F stand for gravitational body force and external force, and τ symbolizes stress tensor represented by the equation below:

$$\tau = \mu[\left(u_i u_j + u_i u_j^T\right) - \frac{2}{3}\nabla.u_i I \tag{3}$$

Here I is the unit tensor, μ is molecular viscosity and the term by the extreme of the right is the accounts for volume expansion. Applying the long-time averaged method, the second equation can be transposed into the following Reynolds-averaged Navier-Stokes (RANS) equation:

$$\frac{\partial}{\partial t}(\rho u_i) + \frac{\partial}{\partial x}\left(\rho u_i u_j\right) = -\frac{\partial p}{\partial x} + \frac{\partial}{\partial x}\left\{\mu\left[\left(\frac{\partial u_i}{\partial x_j}\right) + \left(\frac{\partial u_j}{\partial x_i}\right) - \frac{2}{3}\partial_{ij}\frac{\partial u_j}{\partial x_j}\right]\right\} + \frac{\partial}{\partial x_j}(-\rho u_i u_j) \tag{4}$$

The relation of velocity gradient with Boussinesq hypothesis for the Reynold's stresses, $-\rho u_i u_j$ in the above equation is as follows:

$$-\rho u_i u_j = \mu_t\left(\frac{\partial u_i}{\partial x_j} + \frac{\partial u_j}{\partial u_i}\right) - \frac{2}{3}(\rho k + \mu_t\frac{\partial u_k}{\partial x_k})\sigma_{ij} \tag{5}$$

Molecular velocity due to stress tensors is represented as σ_{ij}.

Species conservation equation

$$\nabla.(\rho u_i Y_i) = -\nabla.\vec{J_i} + R_i \tag{6}$$

Where $\vec{J_i}$ is the diffusion flux term of species i.

3.1.2 Turbulence model

The k-model in this work was able to solve the flow field inside the furnace using a Reynolds averaged term with ease. The realizable k- ε model, which simulates turbulence, uses a different formulation for the turbulent viscosity and a modified transport equation for the dissipation rate that was obtained from the exact transport equation of the mean-square vorticity fluctuation. Equations 7 and 8 below illustrate the modeled transport equations for k and ε.

k equation

$$\frac{\partial}{\partial x}(\rho k) + \frac{\partial}{\partial x}(\rho u_i k) = \frac{\partial}{\partial x_j}[\left(\mu + \frac{\mu_t}{\sigma_k}\right)\frac{\partial k}{\partial x_j} + G_k - \rho\varepsilon \tag{7}$$

ε equation:

$$\frac{\partial}{\partial t}(\rho\varepsilon) + \frac{\partial}{\partial x}(\rho u_i \varepsilon) = \frac{\partial}{\partial x_j}[\left(\mu + \frac{\mu_t}{\sigma_\varepsilon}\right)\frac{\partial \varepsilon}{\partial x_j} + C_{1\varepsilon}\frac{\varepsilon}{k}G_k - C_{2\varepsilon}\rho\frac{\varepsilon^2}{k} \tag{8}$$

$$\mu_t = c_\mu \rho \frac{k^2}{\varepsilon}$$

The generation of kinetic energy and buoyance force attribution are:

$$G_k = -\rho u_i u_j \frac{\partial u_j}{\partial x_i} \tag{9}$$

$$G_b = \beta g_i \frac{u_t}{Pr_t}\frac{\partial T}{\partial x_i} \tag{10}$$

The turbulent dissipation rate (ϵ)

$$\frac{\partial}{\partial t}(\rho\varepsilon) + \frac{\partial}{\partial x_j}(\rho\varepsilon u_j) = \frac{\partial}{\partial x_j}\left[\left(\mu + \frac{\mu_t}{\sigma_\varepsilon}\right)\frac{\partial\varepsilon}{\partial x_j}\right] + \rho C_1 S\varepsilon - \rho C_2\frac{\varepsilon^2}{k+\sqrt{\nu\varepsilon}} + C_{1\varepsilon}\frac{\varepsilon}{k}C_{3\varepsilon}G_b + S_\varepsilon \tag{11}$$

3.1.3 Radiation model

For tracking radiation in the furnace, the discrete ordinate model was applied. At any point in the furnace, the intensity of radiation is represented by:

$$\frac{dl(\vec{r},\vec{s})}{ds} = -kl(\vec{r},\vec{s}) + kl_b(\vec{r}) \tag{12}$$

In equation (12), $\vec{r}$ is any position in the furnace along path $\vec{s}$ through an emitting, absorbing or non-dispersing medium [3]. Also, l represents intensity, l_b represents black body intensity is dependent on local temperature. Deviation in the radiative heat flux is used to show the effect of radiation intensity in the energy equation.

$$-\nabla . q^R = k(4\pi l_b(\vec{r}) - \int_{4\pi} I(\vec{r},\vec{s})|\vec{s}.\vec{n}|d\Omega' \tag{13}$$

3.1.4 Thermal stress model

For the FEA slab thermal stress model the governing equations are:

Stress Vector (σ)

$$\boldsymbol{\sigma} = \boldsymbol{D}(\boldsymbol{\varepsilon} - \boldsymbol{\varepsilon}_T) \tag{14}$$

Where D is the material stiffness matrix, e is the strain vector

Thermal strain vector (ε_T)

$$\boldsymbol{\varepsilon}_T = \alpha(T - T_0) \tag{15}$$

Where α is the thermal expansion coefficient, T_0 is the reference temperature, T is the temperature.

3.1.5 Scale formation model

High-temperature oxidizing combustion gases are present in the reheating furnace and easily react with the steel slabs. As a result, a thin layer of oxidized scale made up of wüstite (FeO), magnetite (Fe_3O_4), and hematite forms on the slab's surface (Fe_2O_3). However, 95% of scale is FeO at temperatures greater than about 600°C. [41]. FeO is the iron oxide on which this study focuses. The rates of oxidation during reheating in the industrial furnace appear to follow a combination of linear and parabolic rate laws, according to the expected scale formation rates utilizing isothermal gas atmosphere [41]. When free oxygen is directly reacted with and adsorbed onto the steel slab surface during steps one and two, a linear rate is produced. The rate at this stage is controlled by surface reaction and oxidant transport and is calculable using a particular rate constant, k_l. This scale will prevent oxidant movement to the slab surface once a thin scale film has grown on the surface of the slab. In steps three and four, the steel ions continue to produce scale by diffusing through the current oxide layer and interacting with free oxygen. Figure 2 illustrates how a parabolic rate law with a particular rate constant, k_p, can be used to describe how solid-state diffusion and grain boundary diffusion govern the rate in this stage.

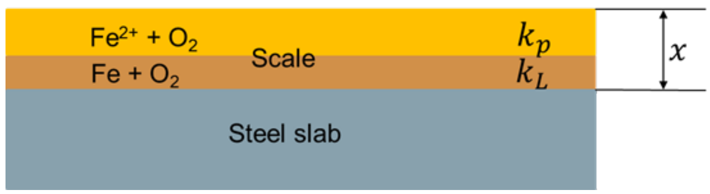

Figure 2. Schematics of scale growth kinetics.

This relationship for the oxidation behavior of steel slabs can be represented as follows.:

$$\frac{1}{k_l}x + \frac{1}{k_p}x^2 = t \tag{16}$$

where *x* is the scale thickness and *t* is the slab residence time.

The rate constants k_p and k_l are based on different properties. The parabolic rate constant formula was derived by is based mainly on scale properties and phase equilibria [37,43]:

$$k_p = 6\frac{\rho_{FeO}^2 M_O^2}{M_{FeO}^2} \cdot D_{Fe^{2+}}^{*}(\gamma_{FeO/Fe_3O_4} - \gamma_{Fe/FeO}) \tag{17}$$

Here, ρ is the density of scale, M is the molecular weight of either oxygen or wüstite, γ signifies the iron ion vacancy concentrations at the boundary specified, and $D_{Fe^{2+}}^{*}$ is the iron self-diffusion coefficient [44]. Himmel et al. found the iron self-diffusion coefficient to follow the equation

$$D_{Fe^{2+}}^{*} = 0.118 \cdot e^{-124,300/RT}. \tag{18}$$

The linear rate constant was derived in three parts using experimental results from Abuluwefa et al. [41], mass transfer principles, and gas properties. The linear rate constant is the summation of the rates of all of the oxidizing species.

$$k_l = M_o(k_{l,CO_2} + k_{l,H_2O} + k_{l,O_2}) \tag{19}$$

$$k_{l,CO_2} = K_{CO_2}(a_O^*)^{-\frac{2}{3}}(1 - \frac{a_O^*}{a_O'})P_{CO_2} \tag{20}$$

$$k_{l,H_2O} = K_{H_2o}(a_O^*)^{-\frac{2}{3}}(1 - \frac{a_O^*}{a_O'})P_{H_2O} \tag{21}$$

$$k_{l,O_2} = \frac{4}{3}\frac{D_{O_2}}{l}Re^{1/2}Sc^{1/3}(C_{O_2}^G - C_{O_2}^*$$

(22)

Here, M_o is the molecular weight of oxygen, a_o is the oxygen activity of wüstite in equilibrium with iron (a_O^*) and in equilibrium with the gas phase (a_O'), P_i is the partial pressure of the species i, Re is the Reynolds number, Sc is the Schmidt number, D_{O_2} is the binary diffusion coefficient of oxygen, l is the effective length of the sample, C_{O_2} is the molar concentration of oxygen in the gas phase (superscript G) and at the interface (superscript *), and K_{CO_2} and K_{H_2O} are the phase boundary reaction rate constants. The values of the oxygen activity were derived from Darken and Gurry[38]. Abuluwefa[22] experimentally found the phase boundary reaction rate constants to be dependent on temperature as $K_{CO_2} = 18{,}490 \cdot e^{-274{,}362/RT}$ and $K_{H_2o} = 28{,}280 \cdot e^{-263{,}555/RT}$.

3.2 Simulation approach

3.2.1 Combustion

A systematic approach was applied to study the transitioning from methane fuel to hydrogen in a reheating furnace. Firstly, a single burner study was modeled for both fuels using CFD software ANSYS FLUENT. Combustion of methane as fuel in the single burner was used the baseline case, Extensive analysis on the associated species distribution, temperature distribution and heat flux profile in comparison to hydrogen under the same operating conditions were conducted. Secondly, to examine flame interactions for both fuels using multiple burners, same comparative analysis was carried out by modeling the bottom intermediate zone from the same furnace. Emission gases, temperature profile and heat flux results were carefully recorded. It is important to note that for the single zone modeling, inter-zonal interactions where not considered. Furthermore, the entire reheating furnace was modeled in which three individual cases below were considered:

- Case 1: Only methane as its fuel source. This case was also used as the baseline case.
- Case 2: In this scenario, the furnace was modeled with methane in all furnace zone burners except for the intermediate zone where there was hydrogen inclusion but of the same heat input value as when methane was used in the zone as a fuel source.

- Case 3: Hydrogen as fuel in the heating zone 2 (the furnace zone which has the highest energy input) while all other zones maintained methane application.
- Case 4: Hydrogen was applied to the all furnace zones

3.2.2 Thermal Stress

A CFD model of a methane fueled walking beam reheat furnace with steel slabs passing through was created and run until the simulation reached steady state. The furnace contains five zones: preheat zone, two heating zones (heat zone 1 and heat zone 2), intermediate zone, and a soak zone. The slabs of the furnace moved through the furnace length of 53.69 m. 41 slabs of width 1.27 m fit within the furnace therefore the time each slab spent in a single position was estimated as 3.5 minutes. The results of the full furnace simulation using methane were validated using industrial thermocouple data and the heat flux profiles on the slabs were generated.

The heat flux values on each slab through the furnace were used successively as the boundary conditions on a single slab for 3.5 minutes at a time in a transient simulation. This generated the current temperature distribution through the slab at its position in the furnace, accounting for the heating history of the slab passing through the furnace. The successive application of heat flux boundary conditions on a single slab accounts for the heating of its previous positions, and generated a separate slab temperature profile for each position within the furnace.

The temperature profiles through the slab at each position in the furnace were then used individually as a thermal load condition in an FEA model of the slab. The thermal stress was then calculated from the thermal load until the stress valued converged, resulting in the current thermal stress results for slabs in each position of the furnace.

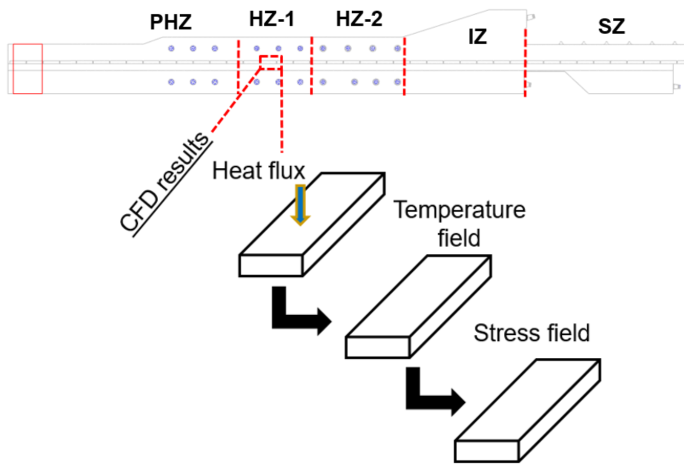

Figure 3. Visual of study methodology.

A baseline simulation was run first using methane as fuel, as is standard in furnace operation. The baseline values for the thermal stress, and their location in the furnace were then validated. The process was then repeated with hydrogen as the fuel for combustion.

The thermal stress values along each slab were plotted along the longitudinal line of the slab, and on the centerline thickness of the slab. A longitudinal cross sectional cut showing the thermal stress location and values are generated for inspection. The H_2 and methane combustion thermal stress results are compared. The H_2thermal stress values compared to maximum allowable stress values to determine if there is damage to the slab.

3.2.3 Scale formation

A novel MATLAB application solution procedure was also developed by Worl et. al. to consider the transient scale formation process in a three-dimensional reheating furnace [3]. The scale prediction application takes inputs of temperature of slab and flue gases at different locations across the slab, length of the furnace, dwell time of the slab in the furnace, molar concentration of oxygen, moisture, carbon monoxide and carbon dioxide in the flue gases. The output of the predictor consists of a 1D plot showing the scale growth for each category of scale and the total amount of scale formed. The predictor also allows users to input data using any of the three different methods namely; manual input method, spreadsheet method or zone input method. These input methods and user interface was modified to allow for flexibility. The model was used to compare the different categories of scales and their growth for both hydrogen and methane fired reheat furnaces.

4. COMPUTATIONAL DOMAIN AND BOUNDARY CONDITIONS

4.1 Single burner

This study was carried out using designs from the walking beam reheat furnace at the Cleveland-Cliffs Indiana Harbor, the geometry of the furnace used for the study is as seen in Figure 1. This study was approached using a systematic process that will be convenient for switching fuels in the steel industry. The burner dimensions are 0.0013^2 and $0.0014m^2$ for the air and fuel ports, respectively. The burner has 12 air inlets of same size for even distribution of the oxidizer for symmetrical flow of combustion gases and the fuel inlet is located at the center of the burner. The mass flow rate for oxygen and air are 0.0061kg/s and 0.2246kg/s respectively when considering the hydrogen case and 0.0146kg/s and 0.2706kg/s for the methane case. The same heat input of 672kW was maintained considering both fuels for the single burner study.

4.2 Furnace Zone

The furnace zone consists of ten identical burners. For each of the burners, the mass flow rate for oxygen and air are 0.0134kg/s and 0.4951kg/s respectively when considering the hydrogen case and 0.0322kg/s and 0.5966kg/s for the methane case. The same heat input of 672kW was maintained considering both fuels for the single burner comparison and 6.72MW for the furnace zone study. It is important to outline that interaction with other furnace zones was not considered for the single zone study. Parametric analysis was also done by varying the equivalence ratio and studying its effect on slab heat flux and NOx emission. The values for the corresponding flow rates and temperatures are tabulated in Table 2. The investigation was carried out using the same furnace zone and only hydrogen was used for this variant equivalence ratio study.

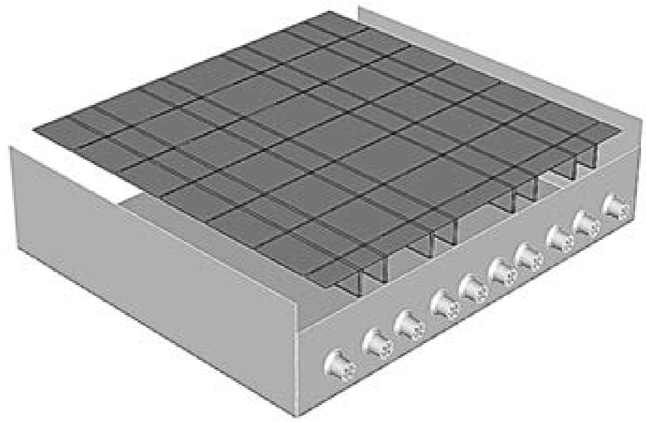

Figure 4. Bottom Intermediate Zone Geometry.

4.3 4.3. Full furnace

In Figure 3, the schematics of the walking beam furnace considered in this study is shown. The study was executed using configurations from the Cleveland-Cliffs Indiana Harbor reheat furnace. A symmetry of the full furnace domain designed using ANSYS workbench software was used for the simulation to save both computational time and cost. The furnace is segmented into five different zones as labelled. Following the movement of the slag along the x axis they are: preheating zone, heating zone 1, heating zone 2, intermediate zone and the soaking zone.

The furnace was designed with twelve preheat burners, twelve heating-1 burners, sixteen heating 2 burners, thirty-six top soak burners and eleven bottom soak burners. The burners used were swirl burners which have one fuel inlet, four primary air inlets and eight secondary air inlets. Flue gas from the furnace leaves from the burner outlet located on both sides of the furnace before the preheat zone. The dimensions of the furnace are 53.69m by 11.96m by 7.6m and for the slabs 1.27m by 7.79m by 0.24m. For the steady state simulation, a total of 40 slabs were in the furnace. Figure 4 shows a tetrahedral meshed surface of a portion of the furnace (top soak zone). A total heat input of 161 MWh was maintained for both fuel cases. The furnace was adequately meshed with about 11 x 10^6 cells.

Slabs travel from the charge door, step wisely through the discharge door. Since it is a walking beam furnace, the slabs do not touch rather, slabs are conveyed by translational beams that move a specific distance dropping the slab at the next location inside the furnace after which the beams return to their previous positions. In the furnace the bottom soak zone has no burners but instead a hearth. Reheat furnace operating conditions entails that fuel is combusted with air or oxygen, as the case may be, and the heat thereby generated in the furnace. However, for both simplicity and accuracy of the model, regions of gas mixtures and heat generation were modeled while tubes and other complex geometries were neglected.

Combustion of natural gas was considered for the baseline case. In this case, a two-steps reaction mechanism was used to model the combustion of natural gas [28]. Moreover, works of Yin and Yinhe, [29] showed that the global hydrogen-air mechanism was in good agreement with complex hydrogen-air mechanism when compared in a combustion test facility. So, for this work, the global hydrogen-air mechanism was utilized to simulate hydrogen combustion in the furnace. The parameters of both reacting mechanisms are listed in Table 1. It is also important to note that for this work, the temperature of the slabs where pre-assigned using industrial temperature data.

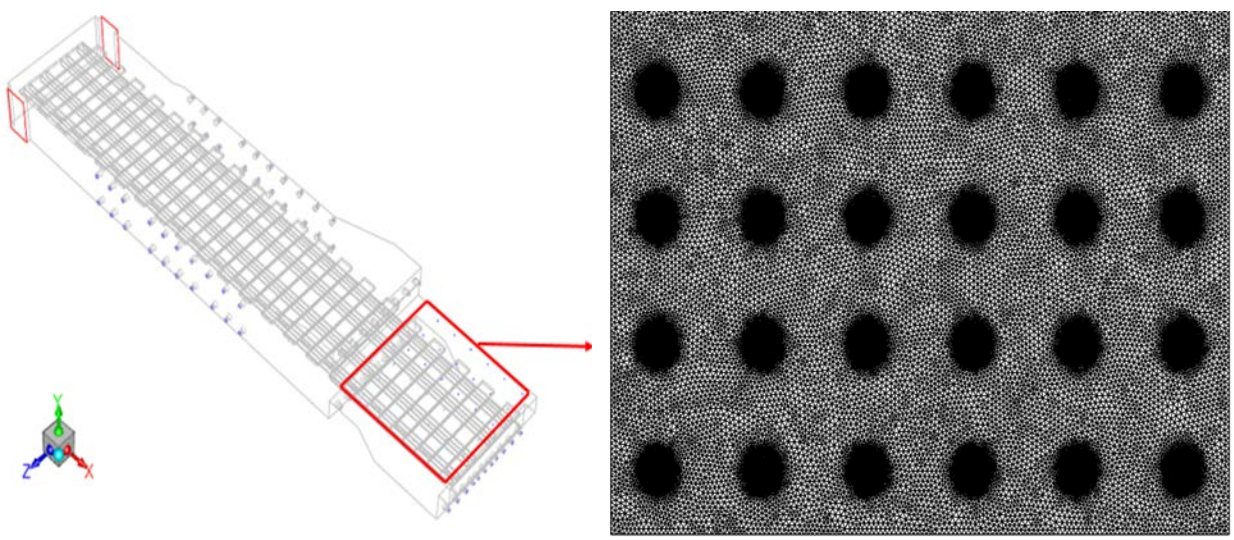

Figure 5. A three-dimensional computational model and mesh.

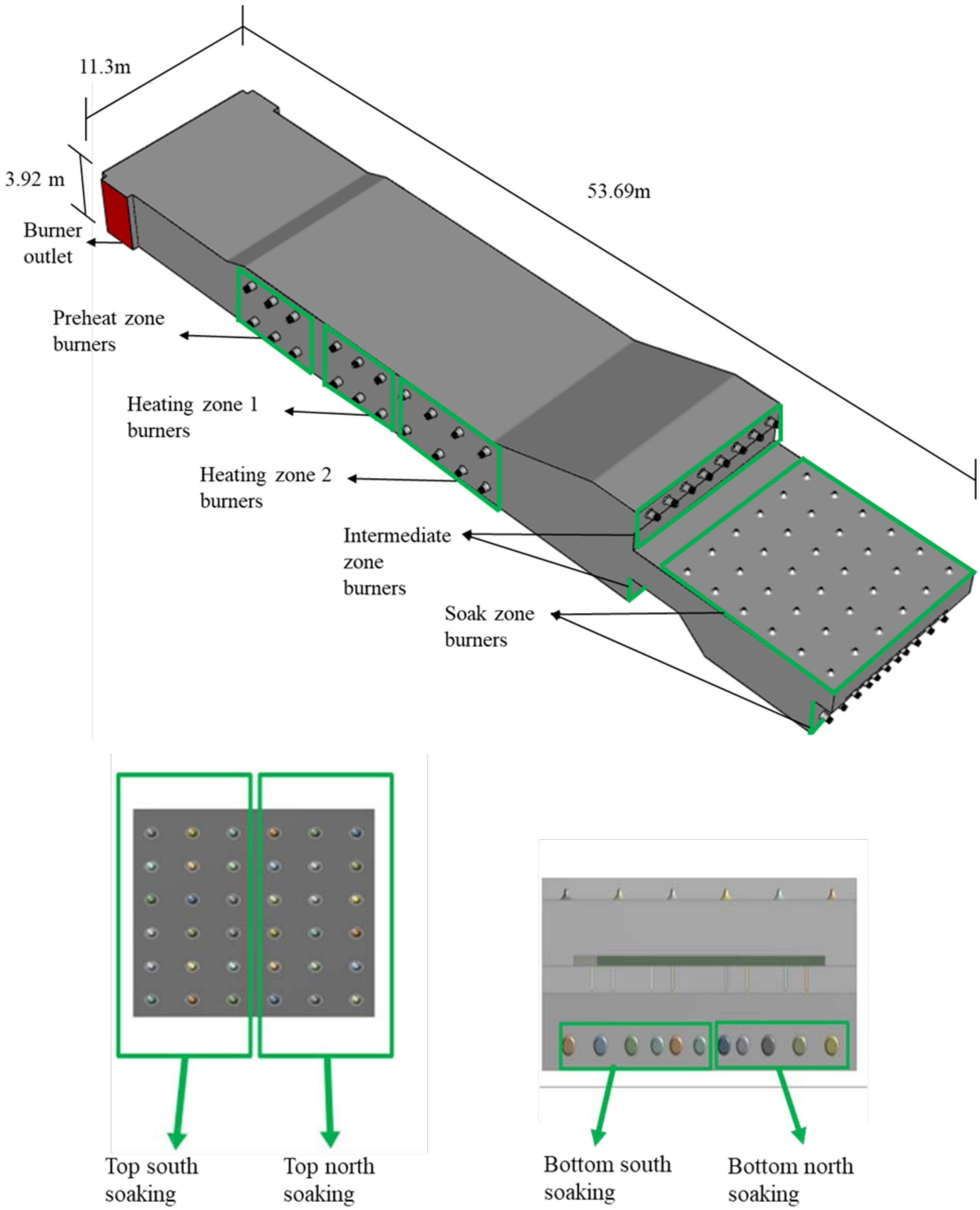

Figure 6. Furnace schematics.

Table 1. Reaction mechanism for fuels.

Reactions	Pre-exponential Factor A (1/s)	Activation Energy E (J/mol)
$CH_4 + 3/2\ O_2 \rightarrow CO + 2\ H_2O$	5.012×10^{11}	2.0×10^{8}
$CO + 1/2\ O_2 \rightarrow CO2$	2.239×10^{12}	1.7×10^{8}
$H_2 + 1/2\ O_2 \rightarrow H_2O$	9.87×10^{8}	3.1×10^{7}

Table 2. Air and fuel flow rates for Natural gas case.

Zone	Methane mass flow rate (kg/s)	Methane temperature (K)	Air mass flow rate (kg/s)	Air temperature (K)
Preheat zone top	0.05	300	0.80	640
Preheat zone bottom	0.05	300	0.90	640
Heat zone 1 top	0.33	300	6.74	640
Heat zone 1 bottom	0.44	300	8.11	640
Heat zone 2 top	0.56	300	11.23	640
Heat zone 2 bottom	0.60	300	11.15	640
Intermediate zone top	0.26	300	4.76	640
Intermediate zone bottom	0.32	300	5.98	640
North soak zone top	0.05	300	1.11	640
North soak zone bottom	0.06	300	1.30	640
South soak zone top	0.05	300	1.20	640
South soak zone bottom	0.11	300	2.09	640

Table 3. Species mass fraction for natural gas.

Species	Air	Fuel Gas
O_2	21%	-
N_2	79%	6.34%
CO2	-	2.40%
CH_4	-	91.26%

In the furnace simulation using hydrogen, the fuel flow rate was adjusted according to its corresponding heating values (161 MWh) so that the heat input of natural gas case was matched, and the air flow rate was recalculated according to the baseline equivalence ratio.

Table 4. Air and fuel flow rates for hydrogen case.

Zone	Fuel mass flow rate	Fuel temperature	Air mass flow rate	Air temperature
	(kg/s)	(K)	(kg/s)	(K)
Preheat zone top	0.009	300	0.305	640
Preheat zone bottom	0.009	300	0.345	640
Heat zone 1 top	0.059	300	2.145	640
Heat zone 1 bottom	0.077	300	2.864	640
Heat zone 2 top	0.100	300	3.664	640
Heat zone 2 bottom	0.105	300	3.918	640
Intermediate zone top	0.100	300	1.723	640
Intermediate zone bottom	0.055	300	2.095	640
North soak zone top	0.009	300	0.359	640
North soak zone bottom	0.009	300	0.409	640
South soak zone top	0.009	300	0.359	640
South soak zone bottom	0.009	300	0.359	640

Table 5. Species mass fraction for hydrogen case.

Species	Air	Fuel Gas
O_2	21%	-
N_2	79%	-
CO2	-	-
H_2	-	100%

5. RESULTS AND DISCUSSIONS

5.1 Validation

5.1.1 Single burner

The numerical model used for this research was validated by comparing flame lengths relative to methane from an experimental study recorded in the works of Turns [17]. Turns recorded in his study that at equal inlet velocity of combustion fuels using a circular port, stoichiometric condition and assuming same mean diffusivity, hydrogen flame length is about one-third of that of methane. Maintaining the same assumptions as listed above using an axisymmetric.

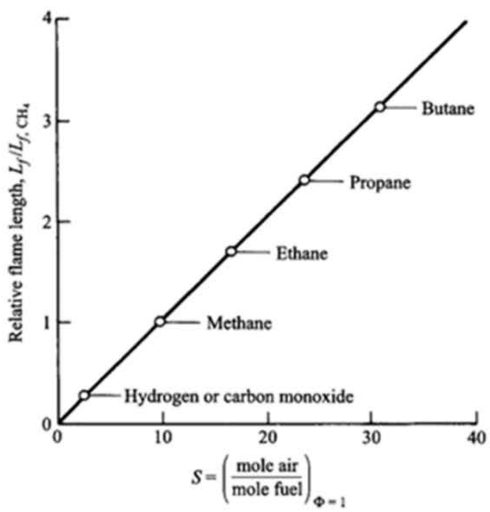

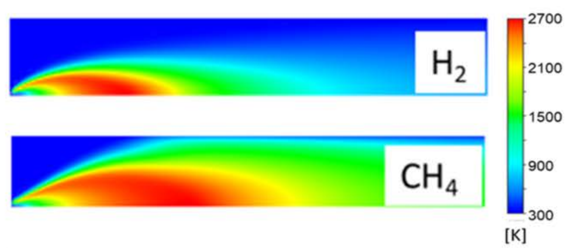

	Methane Flame length	Hydrogen Flame length
Experimental result	1	0.3
Simulation Result	1	0.5

Figure 7. Hydrocarbon fuel flame length relative to methane

5.1.2 Full furnace

The Temperature measurements taken on a reheating furnace at Cleveland-Cliffs using 9 thermocouples positioned as depicted in Figure 7 below were used to validate the full furnace simulation and the results including percentage variance can be seen in the Table 6 and Figure 8 below.

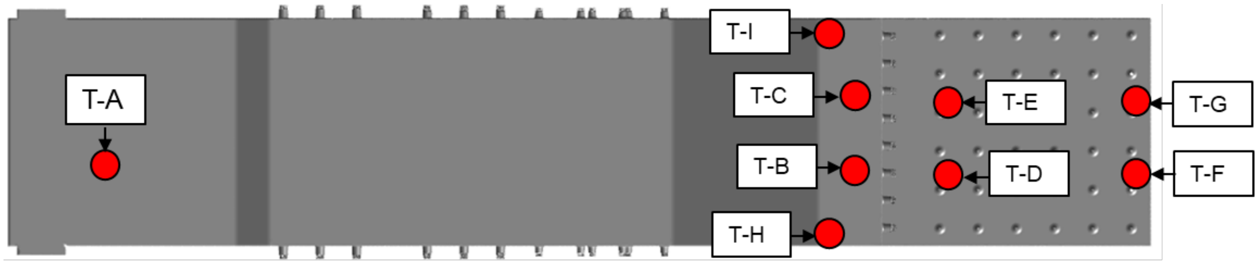

Figure 8. Thermocouple positions in the reheat furnace.

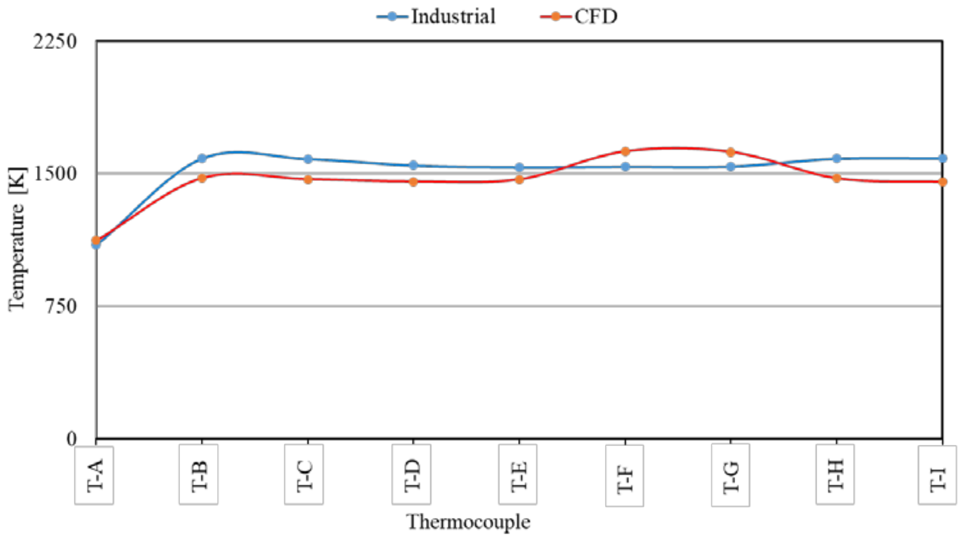

Figure 9. Validation plot for CFD and industrial thermocouple values.

Table 6. Comparison between simulation and thermocouple measurements.

No.	Industrial (K)	CFD (K)	Difference (%)
T-A	1096	1122	2.4
T-B	1587	1475	7.6
T-C	1584	1469	7.8
T-D	1547	1456	6.3
T-E	1537	1468	4.7
T-F	1540	1626	5.6
T-G	1541	1623	5.3
T-H	1586	1474	7.6
T-I	1588	1453	9.3

Thermocouple reading was within 7.2% match with industrial data. This was acceptable for the study.

5.2 Single burner results

5.2.1 Temperature

For the single burner analysis, the burner was tested in open air. For fair comparison, the same burner specification was used as well as the same heat input of 672kW for both the hydrogen and methane cases. As a result of maintaining same heating value, the mass flow rate for hydrogen was lower due to its higher heating value. The values for the temperature plots in Figure 9 extracted from the mid-line that runs through the center of the burner axially.

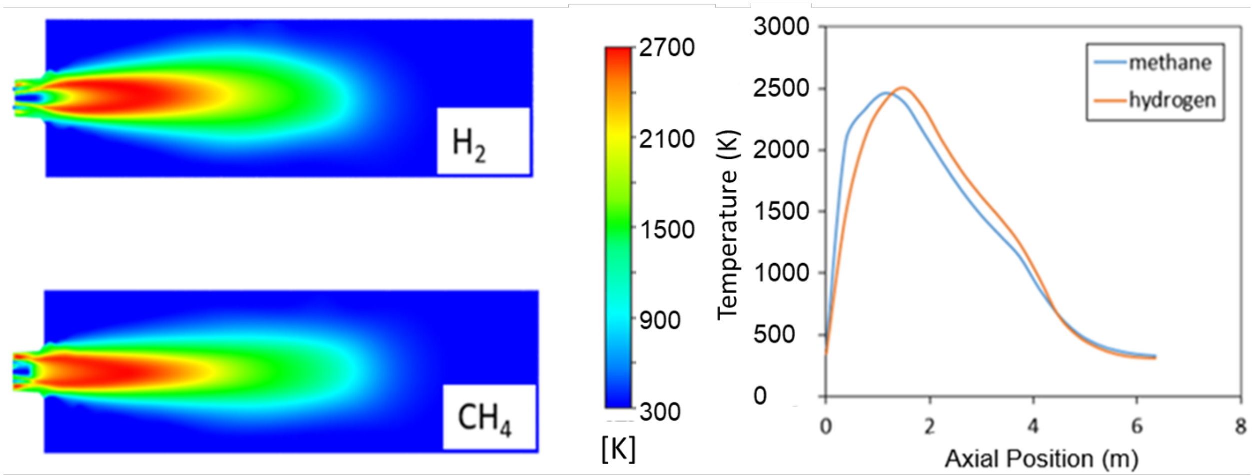

Figure 10. Single burner temperature plots.

It is interesting to note that although the temperature profile for both cases seemed similar, the hydrogen case was wider radially and achieved the highest temperature of 4187ºF, which is about 100ºF higher than methane. From the plot, we can see that hydrogen attained the highest temperature and maintains it until both temperature profiles converged together. For the methane case combustion is seen to take to take place closer to the fuel inlet port and this is due to its low emission velocity into the combustion region as we maintained same heat input.

5.2.2 Fuel velocity analysis

The hydrogen inlet velocity was about 4 times higher than methane inlet velocity. This can be seen from the velocity plot in Figure 10, where the red region signifies high fuel inlet velocity.

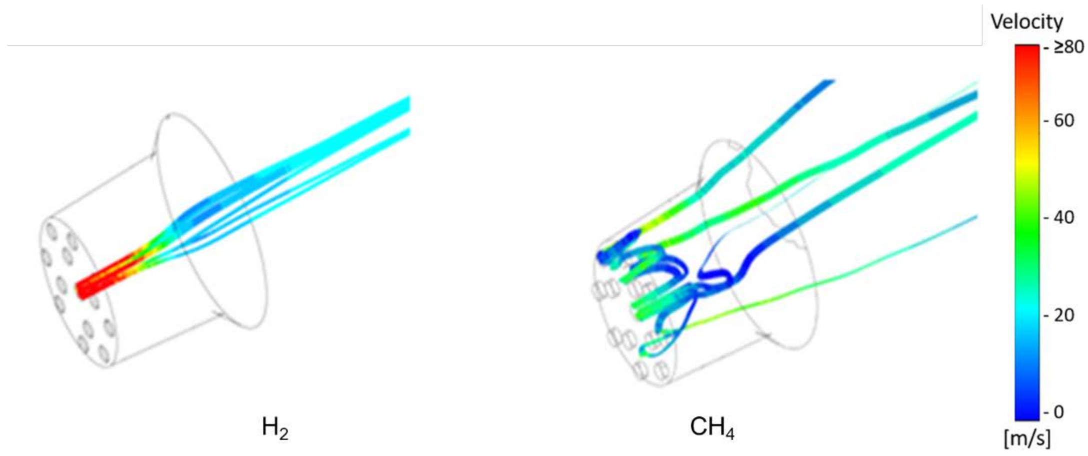

Figure 11. Velocity contours for single burner comparison.

5.2.3 Species distribution

Analysis on species concentrations distributed axially along the combustion domain is shown in Figure 11. The dotted lines represent distribution from the hydrogen case while the continuous lines methane. Carbon-monoxide and carbon-dioxide, represented by the continuous green and red lines respectively, was recorded for the methane combustion while none was seen for the hydrogen combustion. This is a result of the carbon atoms present in methane and absent for the hydrogen.

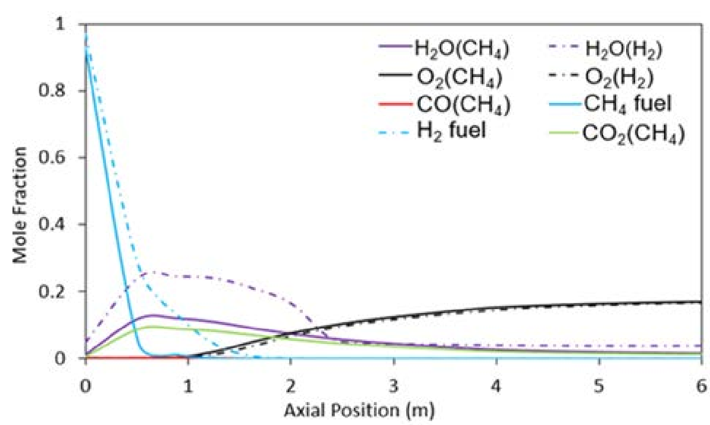

Figure 12. Species distribution plot for single burner.

5.3 Bottom intermediate furnace zone results

5.3.1 Temperature

The visual representations of the flame profiles for each of the fuels while being applied in the bottom intermediate zone are shown in Figure 13. As is the case of the single burner, the flame lengths are still almost the same, although the hydrogen combustion flames are wider and of slightly higher temperature than the methane case

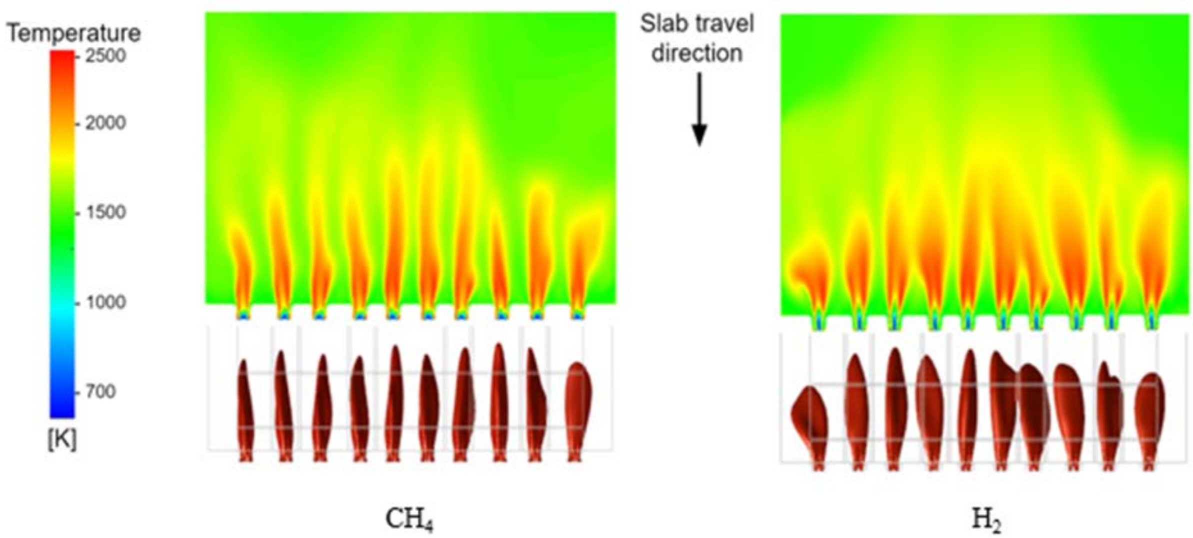

Figure 13. Flame profile in the bottom intermediate zone.

5.3.2 Heat flux

Shown here is the slab heat flux profile plotted for both cases. The result shows a similar heat flux pattern with peak heat flux at the center for each of the scenarios modeled. However, the magnitudes differ for both cases. Hydrogen application shows a higher magnitude of heat flux and this is the result of higher combustion temperature for hydrogen.

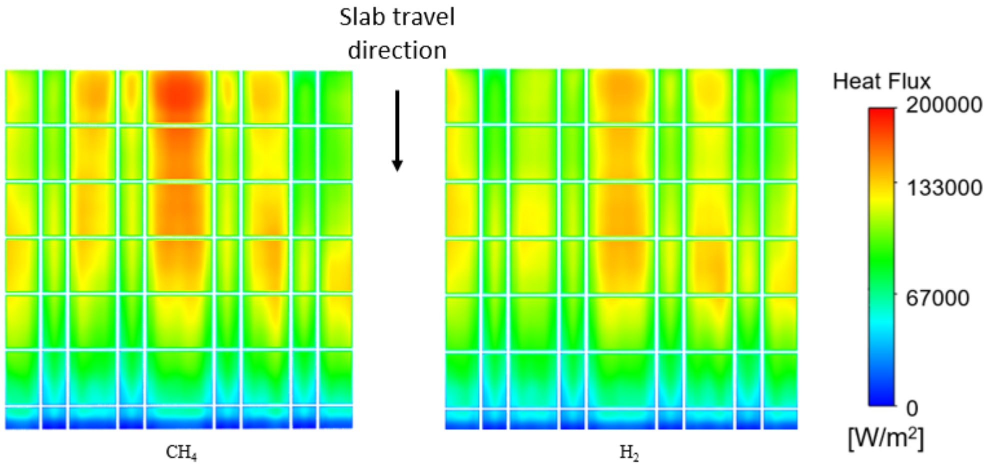

Figure 14. Heat flux profile near slab surface.

Average heat flux magnitudes across the slabs were also studied. Values for the heat flux were taken on lines across the bottom intermediate zones and they were labeled from 0-6. Plot 15, shows the average heat flux distribution on the slab bottom surface. Results show that for both scenarios the peak average heat flux across the slab was recorded close to the center of the zone. However, hydrogen combustion showed the maximum average heat flux value of about 114KW/m^2 while methane had a maximum heat flux value of 109kW/m^2. In order to achieve same heat flux magnitude as the methane case, hydrogen injection rate can be reduced.

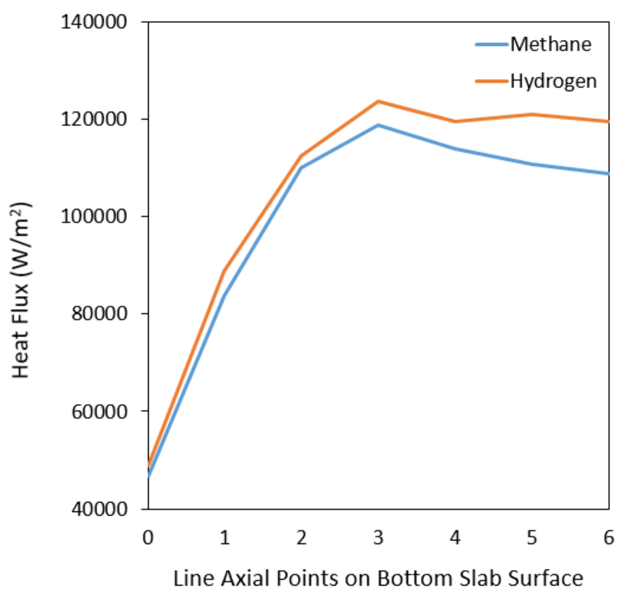

Figure 15. Slab heat flux plot.

5.3.3 Species distribution on slab surface

Calculations for species concentrations near the slab surfaces taking values from the same locations as we did for the heat flux case gave interesting results that are worth taking note of. The values for the concentrations are represented in plot 4. The dotted lines represent the hydrogen scenario while the continuous lines represent the methane scenario. No CO_2 was seen for hydrogen combustion, but it was recorded for methane combustion. Twice the amount of moisture concentration was recorded near the slabs for the hydrogen combustion than for the methane combustion. Studies to see how this higher moisture content can affect scale formation on slabs in a reheat furnace is vital.

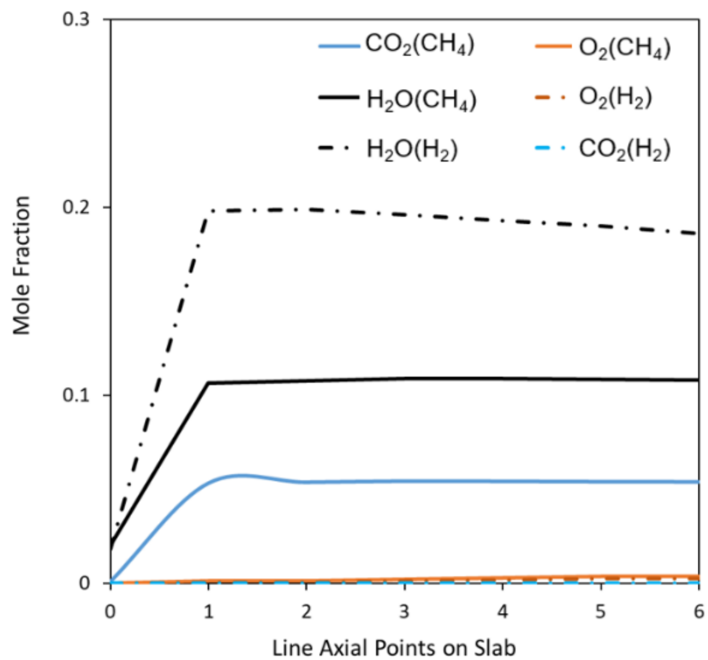

Figure 16. Species concentration plot.

NOx concentration

NOx emission was compared for both methane combustion and hydrogen. As shown in plot 5 it was observed that using hydrogen as fuel emitted a little over twice as much NOx as methane. The high NOx emission for the hydrogen case can be closely attributed to the high temperature seen for hydrogen combustion. Higher temperatures propagate NOx formation. Oxygen enrichment and exhaust gas recirculation should be considered.

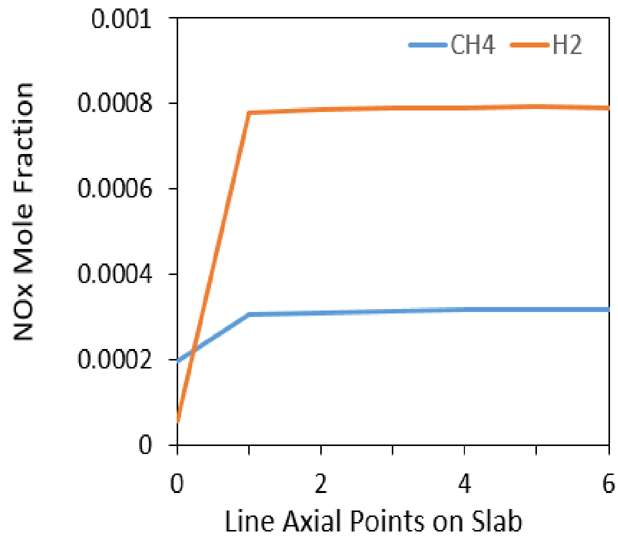

Figure 17. NOx concentration plot.

5.4 Full furnace results

To further analyze the behavior of hydrogen fuel, we used the heating zone 2, which is the zone with the maximum fuel mass flow rate before hydrogen was used as fuel in all the furnace zones. It is also crucial to note that the baseline heat input and equivalence ratios where maintained for all simulations.

5.4.1 Temperature

Comparison of temperature distributions inside the furnace for methane in all zone (Case 1) and hydrogen in the intermediate zone (Case 1) is shown in Figure 17 (a). The overall temperature distributions are similar. Figure 17 (b) shows comparison of temperature distributions inside the furnace for methane in all zone (Case 1) and hydrogen in the heating zone 2 (Case 3). Again, the overall temperature distributions are similar.

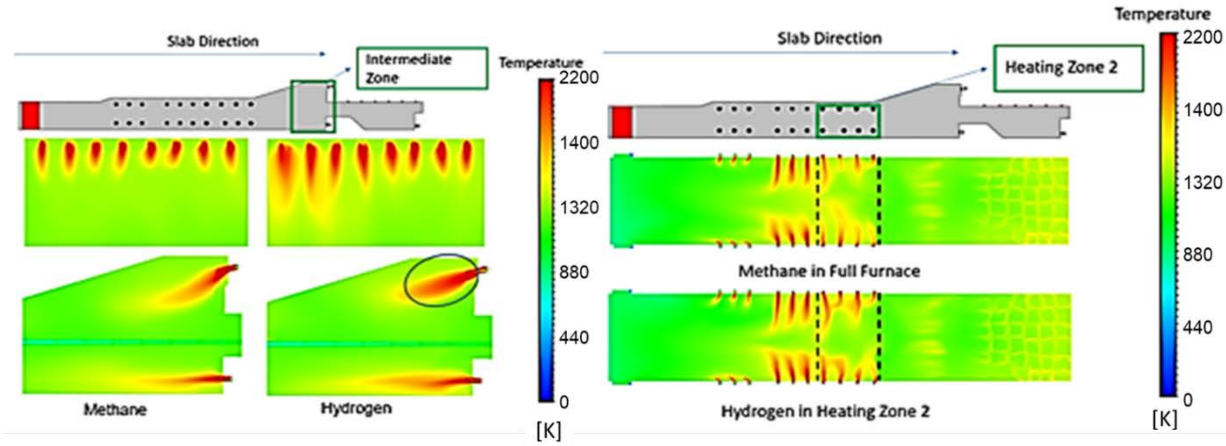

Figure 18. Temperature profile comparison between methane in full furnace application and (a) H_2 in intermediate zone (Case 2) and (b) H_2 in heating zone 2 (Case 3).

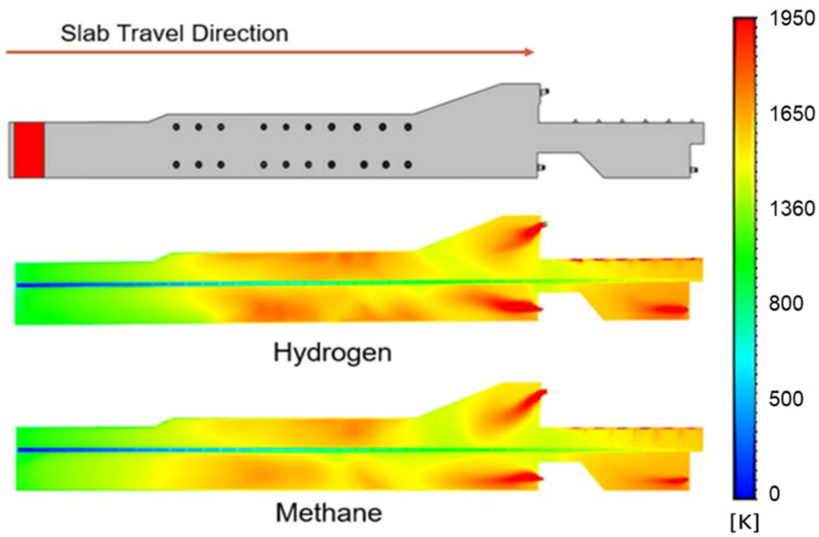

Figure 19. Temperature profiles for hydrogen only (Case 4) and methane only (Case 1).

Temperature on the vertical center plane of the furnace is presented in Figure 18. The hydrogen only application (Case 4) results in 16% more average temperature across the furnace and 17% higher peak temperature for the hydrogen cases when compared with that of methane. This once again reveals that the same trend of higher combustion temperature for hydrogen gas is applicable in the full furnace as seen in this study.

5.4.2 Heat flux

Due to the hydrogen inclusion into different sections of the furnace, it was expedient to study the heat flux profile changes into the slab. This is important to ensure that hydrogen applications yield similar heat flux to the slab as in the methane application and does not create hot spots on the slabs. The heat flux profile for the four scenarios considered in this study is shown in Figure 19.

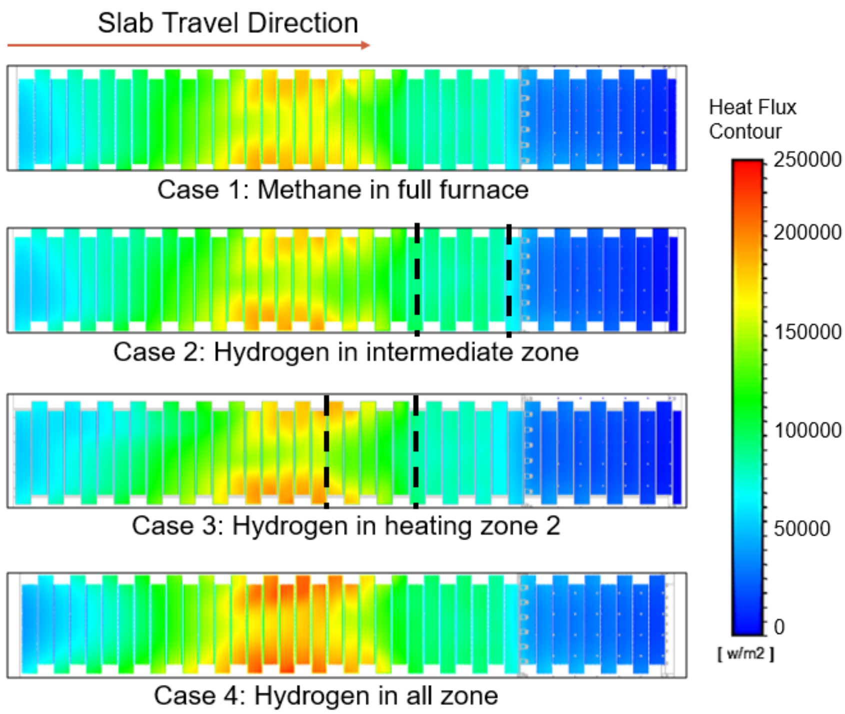

Figure 20. Heat flux into the slabs.

The numerical simulation analysis shows that there was a 0.77% heat flux increase in the heating zone and 6.45% increase in heat flux after hydrogen inclusion in the respective zones. The average heat flux with hydrogen in the entire furnace increased by 6.5%. The higher heat flux recorded in this investigation for all hydrogen cases was as a result of the higher heating value of hydrogen fuel thereby resulting to higher temperature magnitude. However, to avoid any deformations or cracks in this steel slab depending on the steel grade, the temperature parameter can be easily controlled by the following methods.

- Increasing the slab speed in the reheat furnace until the slab heat flux matches the base case heat flux. This way, the slab spends lesser time in the furnace and productivity is thereby increased.
- Reducing the mass flow rate of the hydrogen injection through the burners until similar average furnace temperature as that of the methane case is achieved. Utilizing this technique will not affect the slab dwell time in the furnace and will increase hydrogen fuel savings. Results from this technique is shown in this study.

5.4.3 Species concentration

Hydrogen inclusion has a conspicuous effect on the flue gas composition of a reheat furnace. The hydrogen mechanism used this analysis contained no carbon in its kinetics. This inevitably resulted in lower carbon content when included in the intermediate and heating zones. However, specie like moisture was on the increase with hydrogen as fuel. On the other hand, since moisture is the major product from the combustion of hydrogen, seeing a higher moisture content in the flue gas composition was expected. Below are tabulated values for the flue gas species concentrations.

Table 7. Species concentration at outlet for all cases.

Species	O_2 (ppm)	CO_2 (ppm)	H_2O (ppm)	NOx % increase
Methane Only (Case 1)	0.03	0.076	0.150	-
H_2 in Interm zone (Case 2)	0.028	0.063	0.176	+34
H_2 in Heating zone (Case 3)	0.024	0.049	0.204	+39.5
H_2 Only (Case 4)	0.011	-	0.301	+223

5.4.4 Fluid flow

From the figures below, one sees the impact of the furnace design so that the flue gas leaves in the region just before the preheat zone so that the gas flow is directed towards it. The fluid flow in the furnace is crucial in determining the heating effect on the slab. A rapid change in flow direction, vortices and change in flow velocities modify the temperature distribution and slab heating. The flow pattern of combustion gases across the reheating furnace in both the baseline and hydrogen case is further analyzed in Figures 21 and 22 by showing the velocity contours and streamlines, respectively.

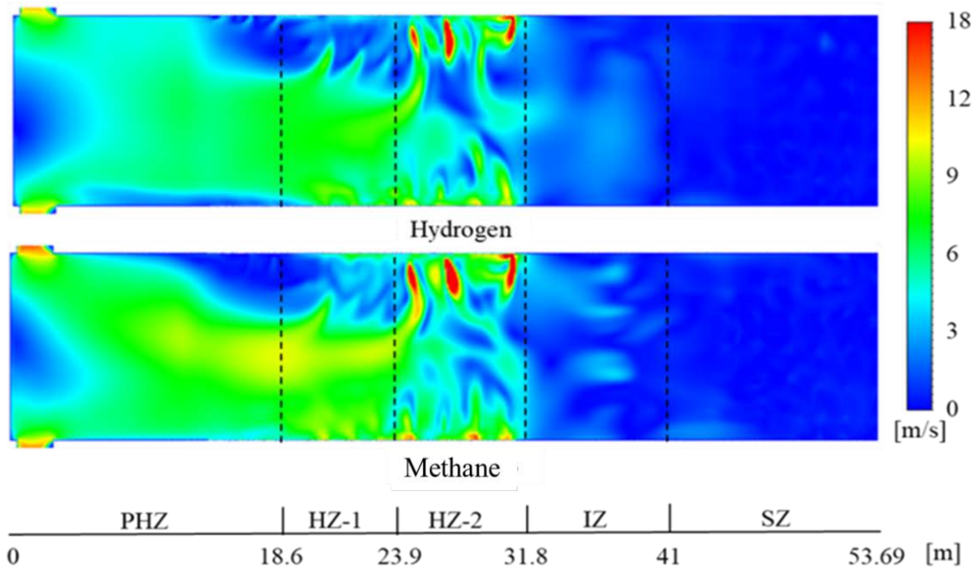

Figure 21. Velocity contour plots.

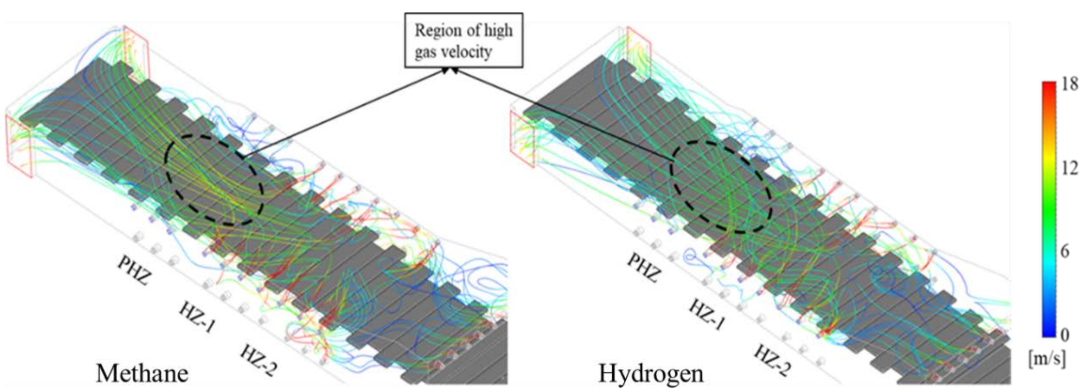

Figure 22. Streamline distribution within furnace.

Results in Figures 21 and 22 reveals similar flow pattern for both fuels in the reheating furnace. However, a higher fluid flow velocity in the heating zone region for the natural gas case than for hydrogen. Also, it can be seen that there is significant difference in flow speed even in the preheating zone and towards the flue gas exit as well. The average flow velocity near the slab surface was 6.1 m/s and 5.61 m/s for natural gas and hydrogen respectively as seen in Figure 22 below.

From Table 2 and 4 above, it can be seen that the total fuel mass flow rate was higher for methane (2.92 kg/s) than hydrogen (1.17 kg/s) which is as result of the higher heating value of hydrogen fuel. These flow rate differences play a major role in the overall flow rate and velocity of the combustion fluid in the reheating furnace. Secondly, moisture has a higher specific heat capacity with respect to temperature when compared with methane. So, as the moisture from the hydrogen combustion moves away from the flame region, it cools faster hence becoming slower towards the exit, which is also seen from the flow velocity plots.

From Figure 21, the fluid flow movement doesn't change significantly. Flue gas recirculation in the reheat furnace aids in adequate distribution of temperature [31] and was observed to occur in both scenarios.

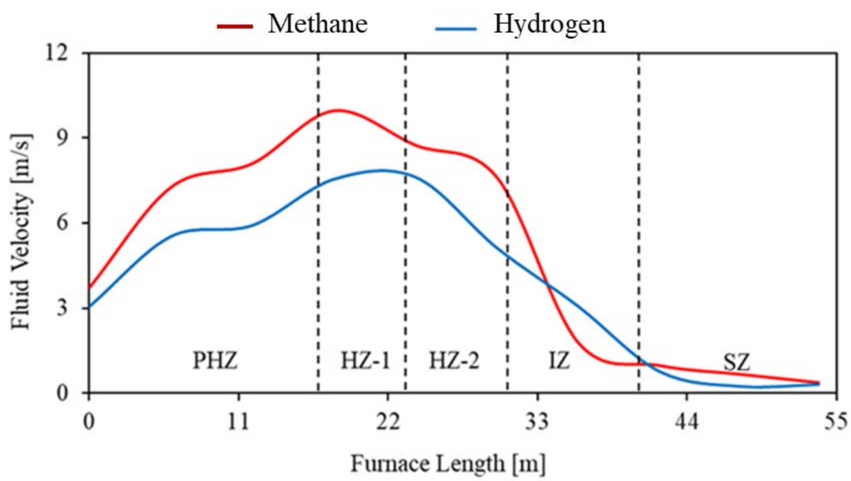

Figure 23. Average velocity plot across the furnace.

5.4.5 Radiative flux

The total surface heat flux into the slabs is a sum of heat fluxes via all the represented mediums of heat transfer and is shown in Figure 23 below for the top surfaces of the slabs. With hydrogen as the primary energy source, 9.62% more average total surface heat flux was recorded to get into the top surfaces of the slab. The average total heat flux for the methane and hydrogen cases are 92177 W/m2 and 99206 W/m2 respectively. Hydrogen utilization showed higher heat flux which can be attributed to the high temperature of hydrogen combustion.

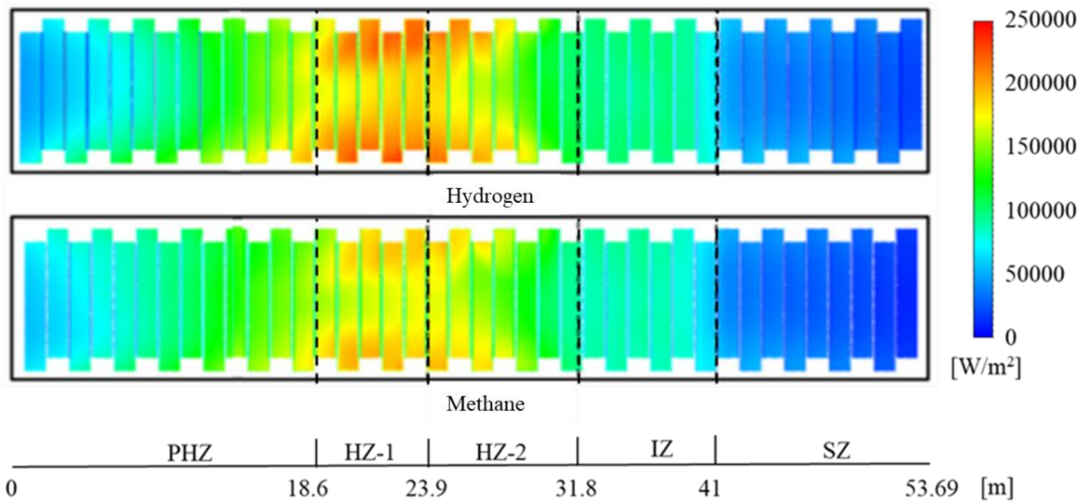

Figure 24. Contours of total heat flux into slabs.

From studies, over ninety percent of the heat flux into the slab in a reheating furnace is a function of radiation. The plot below represents methane radiative heat fluxes into the slab against the total surface heat flux. For this comparative analysis between methane and hydrogen radiation, the effect of skid surface contacts is neglected.

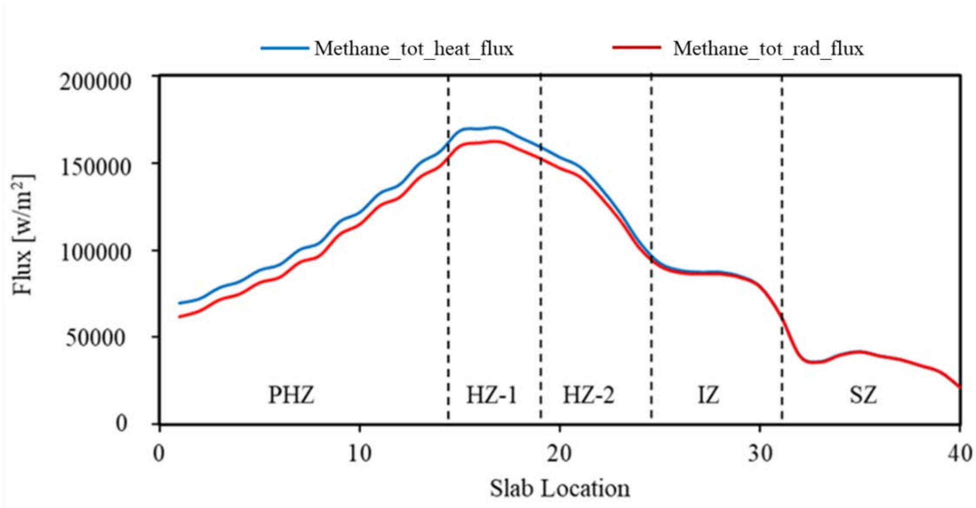

Figure 25 Methane total heat flux vs. radiation flux.

From the methane simulation heat flux plot in Figure 24 radiative fluxes make up 95.3% of the total heat flux into the slabs. These values agree with literature studies [20] of the dominant heat transfer medium in a reheat furnace as radiation when using methane as fuel. The heat fluxes gradient increased steadily in the preheating zone and peaked in the HZ-1. Heat fluxes reduced in the HZ-2 and IZ and leveled off in the soaking zone due to lower heating in the soak zone.

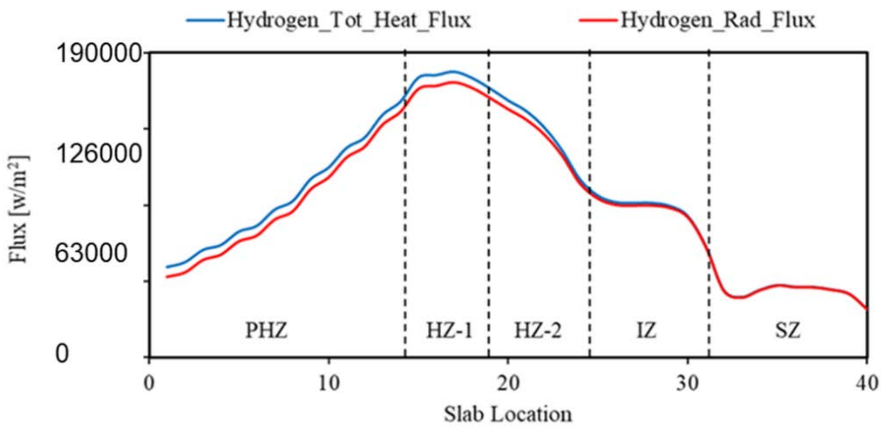

Figure 26. Hydrogen total heat flux vs. radiation flux.

In Figure 25 the total heat flux into the slab is compared to the radiative heat flux. The heat flux profile followed a similar trend to the methane case. The result reveals that 96.3% of the heat fluxes into the slab using hydrogen is through radiation. These simulations demonstrate that hydrogen combustion in a reheating furnace exhibits similar heat transfer characteristics as methane.

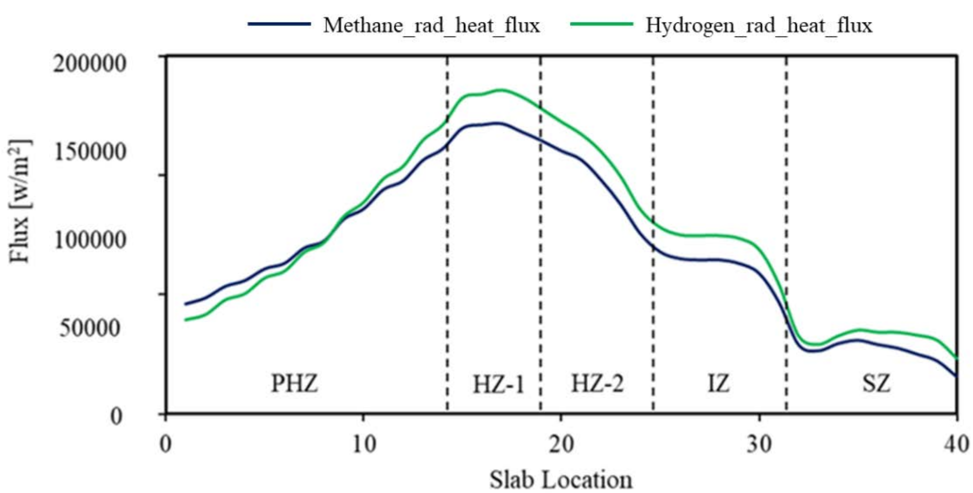

Figure 27. Methane radiation flux vs. Hydrogen radiation flux.

According to the CFD analysis, the average radiation heat fluxes in the reheating furnace was 87887 W/m2 for methane and 95540 W/m2 for hydrogen. Comparing both radiation heat flux distribution in Figure 26 above we can see that although in preheating zone radiation intensity was slightly lower for the hydrogen case, but it peaked at the HZ-1 and HZ-2 which are the heating zones in the furnace and maintained higher radiation levels through the reheating process in the furnace. This also entails that, using hydrogen fuel in the reheating furnace does not negatively affect its primary mode of heat transfer, however it is being optimized in the process.

5.4.6 Thermal stress

Verification

For adequate validation of the thermal stress model that was developed for this study, material properties of the steel material in Ansys workbench was a changed to low carbon steel properties. This was done so the results can be compared with the experimental work of Chen et. al. Density, coefficient of thermal expansion, specific heat capacity, thermal conductivity and young’s modulus were all modified. Chen et.al did an experiment using low carbon steel and discovered that the maximum stress of the steel slab occurred in the slab core between 15 minutes to 20 minutes of heating in the reheating furnace. The maximum thermal stress reached by the slab was about 120 MPa. Figure 27 below shows the thermal stress distribution along the core of the slab and the result shows that the maximum thermal stress of 123 MPa was attained after 14 minutes of slab heating in the reheating furnace. Both the experimental result from Chen et.al. show that low carbon steel slabs reheated using a reheated furnace attains its maximum thermal stress in the preheating zone as a result of the high temperature gradient as they enter into the preheating zone.

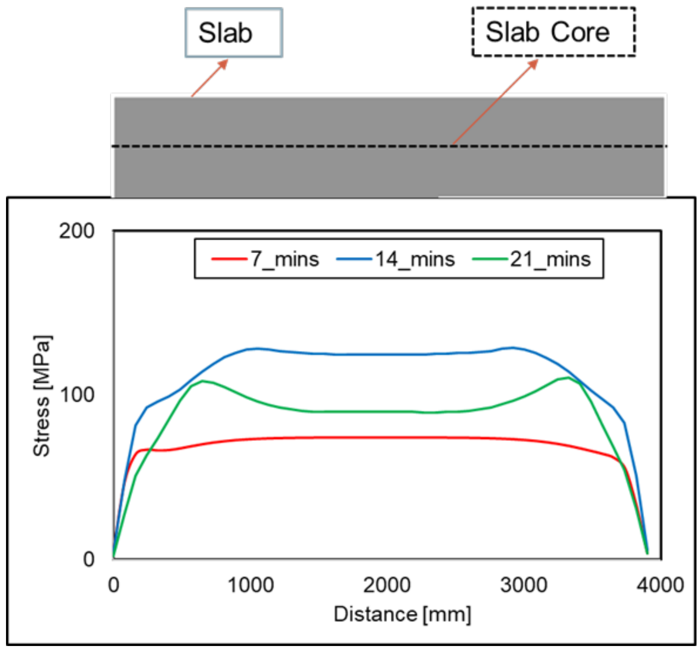

Figure 28. Base case thermal stress distribution.

From our CFD model, the slab stayed a total of 138 minutes in the furnace and this implies that for each position represented in the furnace, the slab was fixed for 3.5 minutes. Stress distribution was studied as the slabs moved from the charge door, through all the zones until it was discharged from the reheat furnace. To properly model this, one slab each was chosen for each furnace zone, this way it will be clear to see the stress variations across all zones as well as the variations in stress patterns as the primary fuel source is substituted.

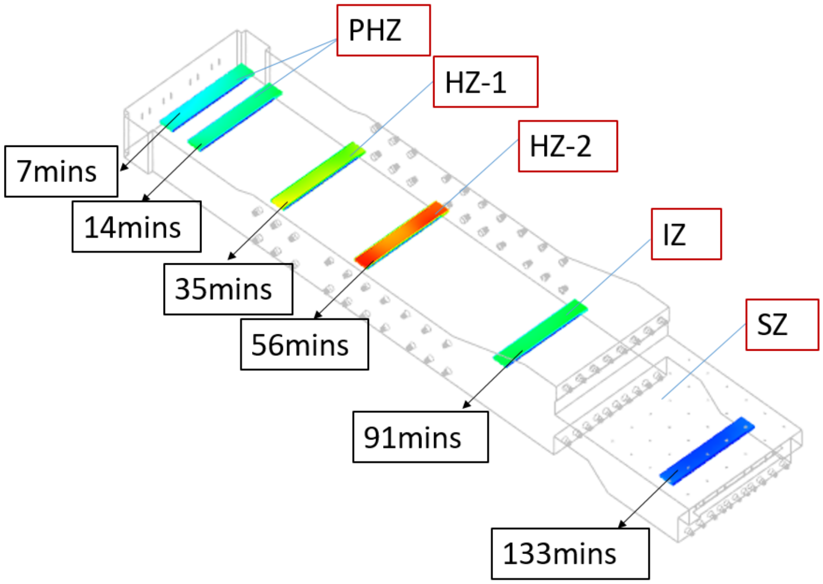

Figure 29. Schematics of selected slabs and their positions in the furnace.

Firstly, we do a visual inspection for all cases we are considering for each slab location in the furnace. Results from the inspection shows stress patterns as the slabs move through the different zones. After 7 minutes of heating the slab in the preheating zone, tensile stresses are seen to develop to a maximum of 116 MPa and 99 MPa in the slab core for methane and hydrogen cases respectively and compressive stresses are seen on the surface of the slab. After 14 minutes of heating, the tensile stress maximum values rose to 123 MPa and 119 MPa respectively. This result also matches the findings of Chen et. al. The tensile stress levels for both by visualizing doesn't seem to be very different, in fact the stress levels seen in the hydrogen case appears to be much safer even though both stress values are well beyond the yield strength values for the steel grade (~168 MPa).

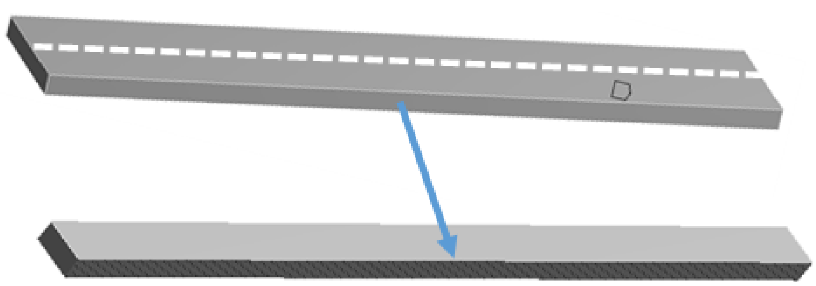

Figure 30. Cross-sectional view for slab stress visual inspection.

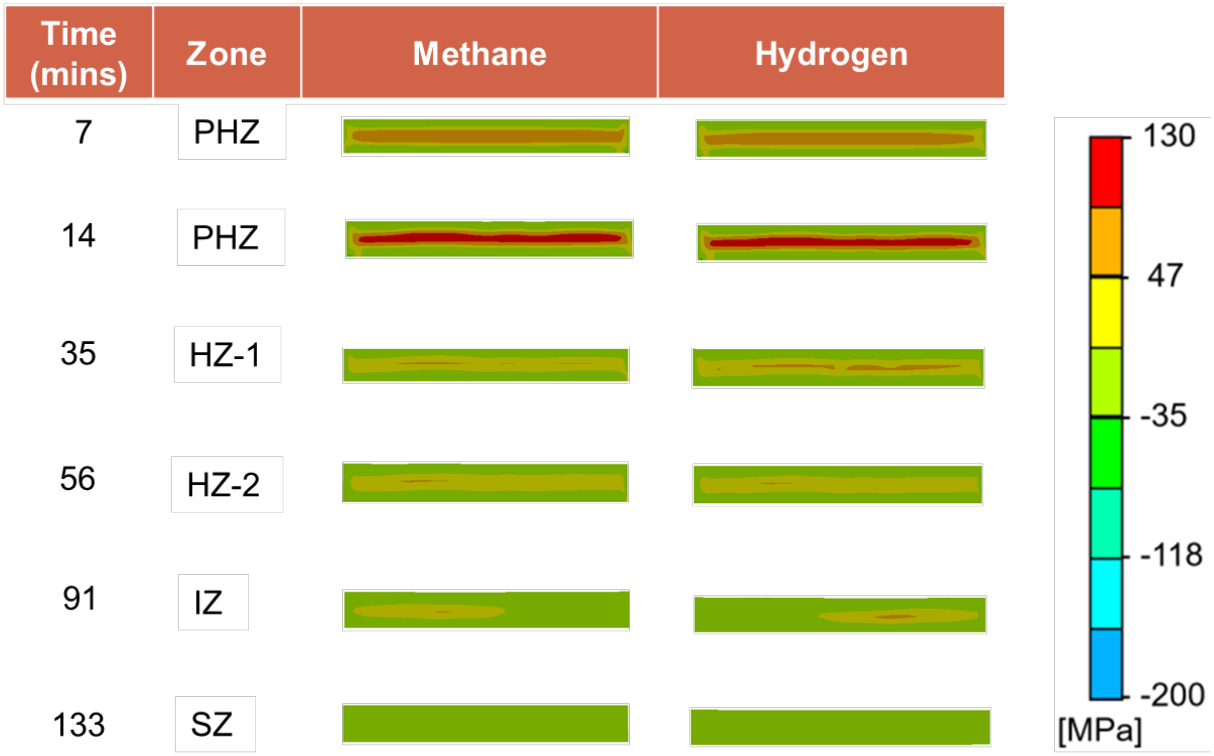

Figure 31. Slab stress contours as it moves through the furnace.

Further detailed analysis was carried out by making plots along the z and y axis of the slab. The y-axis plots show the stress patterns through the middle of the slab from bottom to top as we can see from the Figure 31 below. While, the z-axis plots helped to see the stress patterns along the core length of the slab.

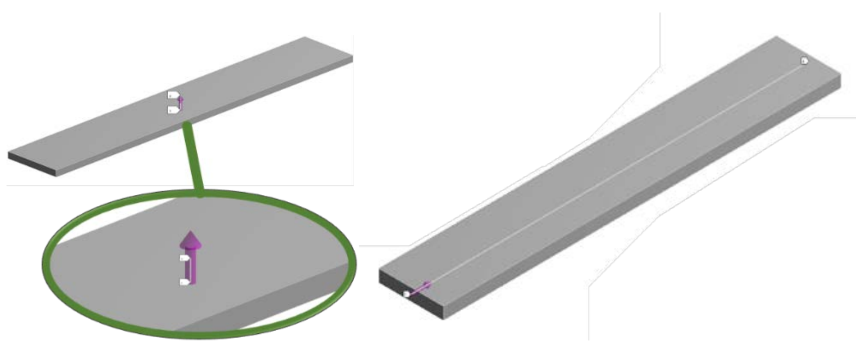

Figure 32. Respective y and z axis paths for stress comparisons.

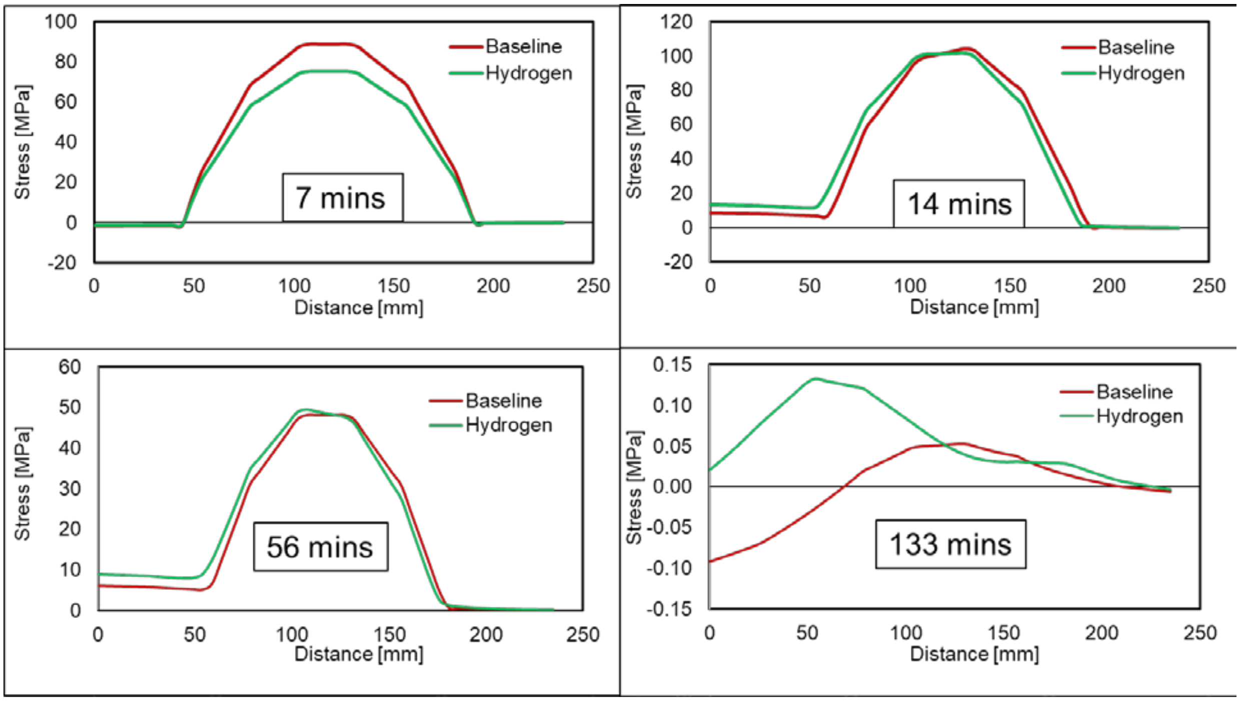

Figure 33. Stress comparison along the y- direction.

Figure 32. shows the stress patterns along the y-axis for the given times shown in the plot. At 7 minutes and 14 minutes the slab was in the preheating zone while at 56 minutes and 133 minutes, the slab was in the heating zone 2 and soak zone accordingly. Just as was earlier visualized, close comparisons were seen for both fuels. The tensile stress picks up after seven minutes and peaks after 14 minutes and then continues to decrease as the slab travels across the reheat furnace until it exits from the soak zone. The maximum tensile stresses for methane and hydrogen are 103 MPa and 102 MPa respectively. When comparing the stresses seen in these two cases, the maximum variation of 14 MPa was observed after 7 minutes of heating as the maximum stress values were 89 MPa for the base case and 75 MPa for the hydrogen case. The stress values are also below the maximum yield stress values for the material at the temperature range. In general, there was no abnormal stress variation from the baseline case that should raise any concern when hydrogen is combusted in the reheat furnace.

The stress plots in Figure 33 below, represents the stress pattern in the core of the slab along the z direction. As the slab moves through the reheat furnace, considering the two scenarios used for this study, no significant difference in tensile stress magnitudes along the z path was recorded for

14 and 56 minutes. At 133 minutes (at the soak zone) the stress differences are almost negligible as they are all near zero values. However, just as we saw in the results along the y-path, the largest stress variation of 14 MPa was seen at 7 minutes with stress values maximum stress values of 89 MPa and 75 MPa for methane and hydrogen respectively. The maximum stress recorded on that path was 111 MPa for both methane and hydrogen cases after 14 minutes.

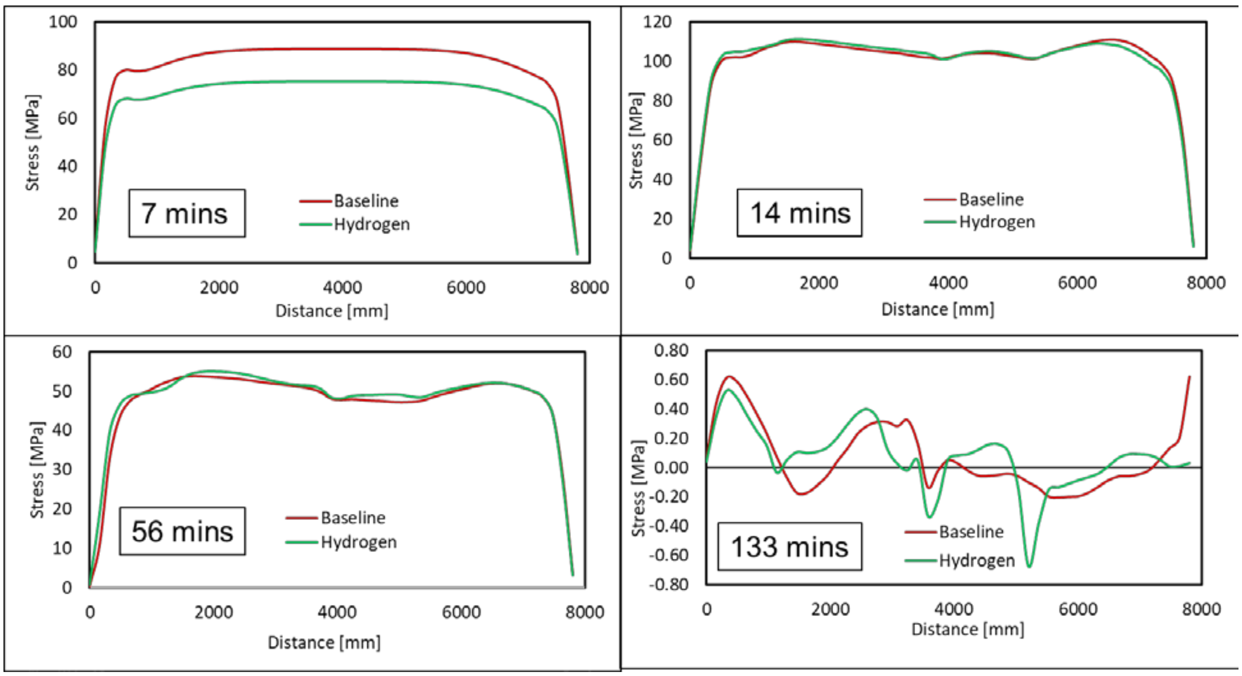

Figure 34. Principal stress comparison along the z-direction.

5.4.7 Scale formation

Scale development was tracked for all scenarios using the scale growth calculator developed with in-house codes that was gotten from the works of Abuluwefa and validated using CFD. The scale analysis showed 11.5% percent increase in scale growth from the baseline case with hydrogen as fuel. A parametric study to investigate the primary factors that contributed mostly to the scale growth showed that the increase in scale growth was as a result of the increase in average gas temperature and moisture in the furnace from the hydrogen combustion. Parameters that were considered for the analysis are namely: gas temperature, furnace length and concentrations of oxygen, moisture and carbon dioxide. Analyzing these various parameters, exposed the major determining factor for the increased scale growth recorded in the hydrogen case.

Table 8. Oxygen molar concentration across furnace for methane and hydrogen.

Distance (m)	(O_2) Methane x 10^{-7} (mol/m^3)	(O_2) Hydrogen x 10^{-7} (mol/m^3)
0	3.955	1.345
0.1556	3.955	1.345
6	3.721	1.10
12	3.392	1.046
18	2.98	8.58
24	2.915	9.42
30	2.786	8.30
36	2.695	8.94
42	3.582	1.017
48	3.452	9.18
53.69	3.417	8.63

Using the scale thickness calculator, the scale thickness for the different fuels were obtained. Results showed a scale thickness of 1.21mm for methane and 1.35mm for hydrogen. The different scale types and their corresponding thicknesses are plotted and tabulated in Figure 34 and Table 9 respectively. From Table 9 we see that the levels of magnetite and hematite for both fuels were approximately similar, however, the increase in scale thickness recorded was primarily more generation of wüstite from the hydrogen fuel giving to 11.5% increase in scale thickness. This makes sense since wüstite is more stable at higher temperatures.

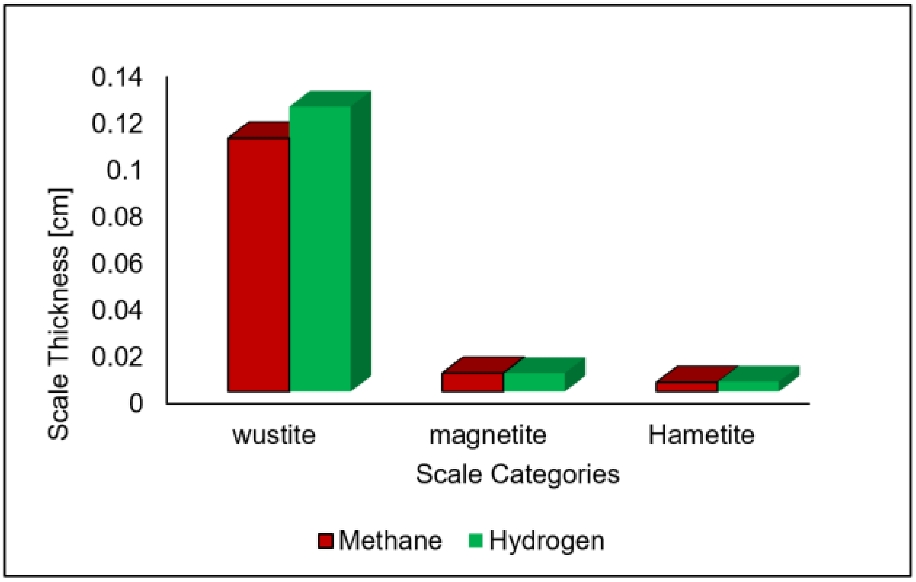

Figure 35. Scale thickness plot for methane and hydrogen.

Table 9. Thickness of the different scale types formed for methane and hydrogen.

Scale Types	Methane (cm)	Hydrogen (cm)
Wustite	0.1087	0.1222
Magnetite	0.008	0.008
Hematite	0.004	0.0043

Effect of species

According to several studies on the parameters associated with the formation of scale, high levels of oxygen are contributory factors to scale development. Species' levels were increased in the furnace by 10%, 20%, 40% and 80% while the temperature in the furnace was kept constant to study its effects on scale. Table 10 shows that oxygen levels contributed more to the scale growth, followed by moisture and carbon dioxide had the least impact. This has also been supported by several literatures to be true.

Table 10. Percentage increase in scale corresponding to increase in species concentration.

% PPM Increase	O_2	H_2O	CO_2
10	3.2	1.0	3.2
20	3.6	2.6	3.2
40	4.5	3.9	3.3
80	6.3	5.8	3.5

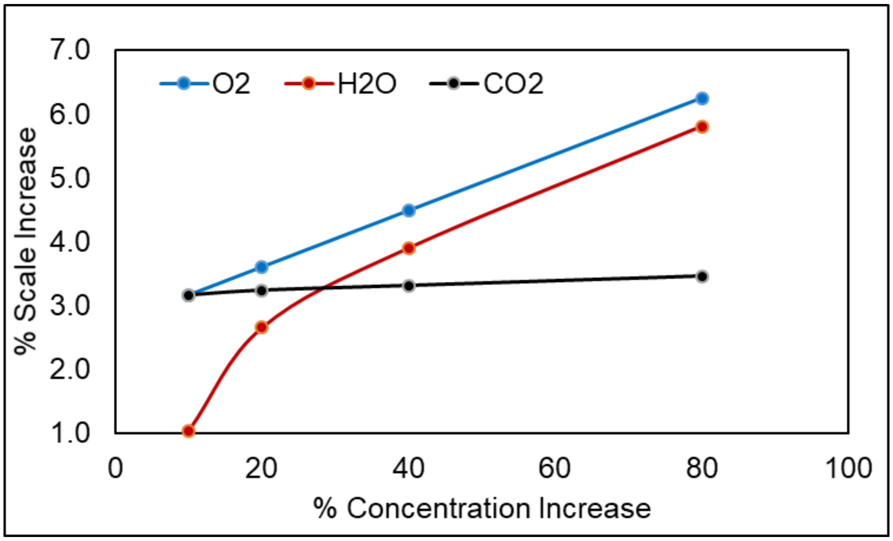

Figure 36. Percentage scale increase plot with increase in concentration of species.

Effect of temperature

To evaluate the effect of gas temperature on the formation of scale, for simplicity, the average furnace temperature for the base case was used as a constant temperature all through the zones as shown in Figure 37. This average temperature was then increased by 1% until 5%. From Table 11 we can see that after a 5% increase in the average gas temperature of the reheating furnace, the scale level rose by 4.34%. This indicates how much of an impact temperature can have on the formation of iron oxides during the reheating process.

Table 11. Gas temperature distribution near the slab.

% Flue Temp. Increase	Average Gas Temp (K)	% Scale Change
0	1359	0
1	1373	+0.4
2	1386	+1.14
3	1401	+2.0
4	1415	+3.0
5	1430	+4.34

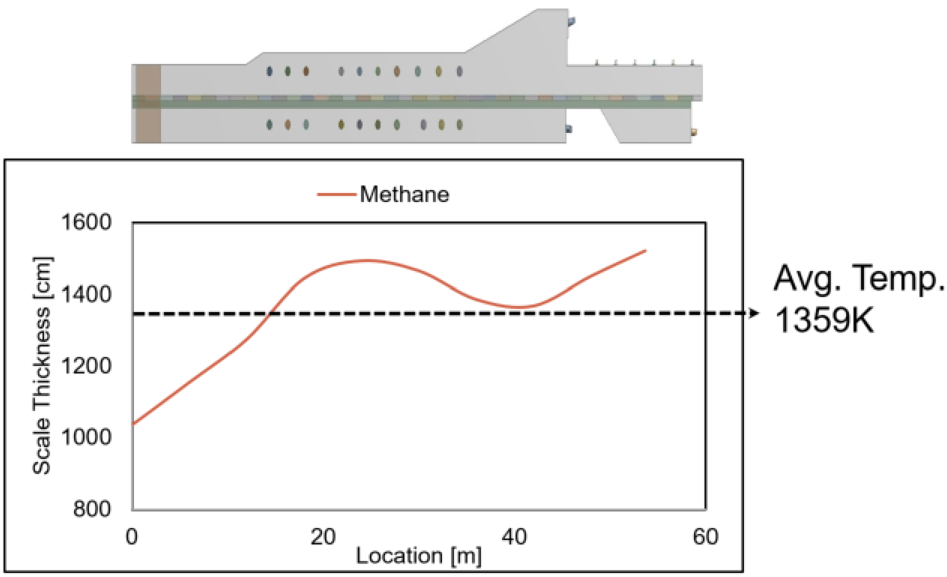

Figure 37. Average furnace gas temperature schematics.

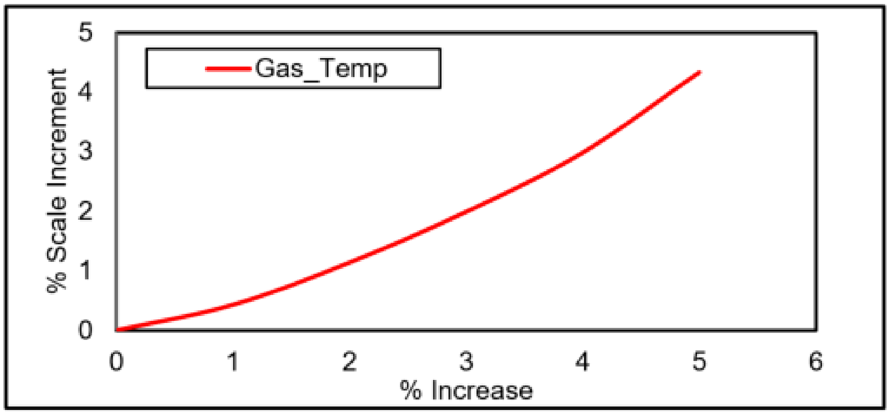

Figure 38. Scale percentage increase plot for temperature change.

Figure 39 is an image of the scale thickness predictor's graphical user interface (GUI). The interface shows the three input options namely: manual input, spreadsheet import and zone input options. For the manual input option, the user inputs the values of the parameters manually into the computer and hits the computer button to receive a scale prediction plot. For the spreadsheet method, an excel spreadsheet is used to input parametric values in the format shown in Table 12. This option is not only more convenient than the manual input, it is also more accurate since it can account for input value from various lengths of the furnace. The last method is the zone method, where the user will need to input the air-furl ratio, zone length, zone average gas temperature and the slab exit temperature of each of the zones represented in his/her reheating furnace. The zone method can give a good estimate and its more suitable for operations where the actual flue gas concentration is not available for input.

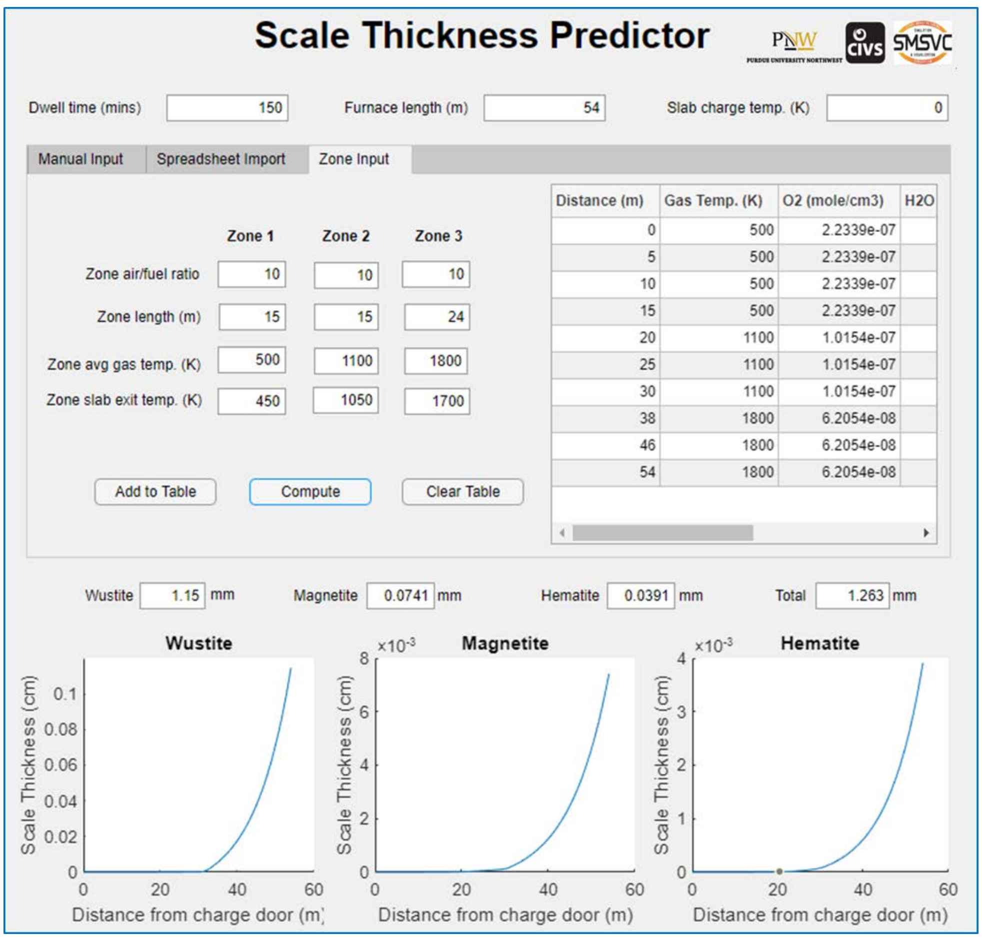

Figure 39. Scale thickness calculator showing results for the different categories of scale.

Table 12. Spreadsheet format used for the scale calculator input.

Distance (m)	Gas Temp (K)	O_2 (x 10^{-7} mol/m^3)	H_2O (x 10^{-7} mol/m^3)	CO_2 (x 10^{-7} mol/m^3)	Slab temp (K)
0	1038	3.955	18.367	9.272	298
0.1556	1038	3.955	18.367	9.272	298
6	1154	3.721	16.382	8.27	418
12	1275	3.392	14.838	7.49	568
18	1444	2.985	13.094	6.61	688
24	1493	2.915	12.633	6.377	838
30	1465	2.786	13.07	6.598	958
36	1386	2.695	14.015	7.075	1108
42	1368	3.582	13.424	6.776	1228
48	1450	3.452	12.6	6.361	1378
53.69	1521	3.417	11.897	6.006	1498

5.5 Techniques to optimize hydrogen application

5.5.1 Reducing hydrogen fuel flow rate

In cases where heat flux into the slab has to be controlled to prevent any form of thermal damages on the steel slab, one option that can be explored is hydrogen fuel flow rate reduction. In this study, the fuel flow rate for the hydrogen case was adjusted in separate zones. After several trials, the total heat input into the furnace was reduced by 18.3% across the furnace zones to achieve a similar average temperature distribution across the reheat furnace.

The equivalence ratio was kept the same for all reheat furnace zones. Table 12 shows the respective air and fuel flow rate changes in each zone. It is also important to note that the percentage change of flow rate across the furnace zone varied. Results from the adjusted flow rate case will be discussed, comparing it to the initial hydrogen and methane cases.

Table 13. Adjusted air and fuel flow rates.

Zone	Initial fuel flow rate (kg/s)	New fuel flow rate (kg/s)	Initial air flow rate (kg/s)	New air flow rate (kg/s)
Preheat zone top	0.0181	0.0200	0.6695	0.3340
Preheat zone bottom	0.0205	0.0226	0.7576	0.3780
Heat zone 1 top	0.1283	0.1219	4.7317	2.0408
Heat zone 1 bottom	0.1711	0.1626	6.3147	2.7211
Heat zone 2 top	0.2190	0.1873	8.0815	3.1336
Heat zone 2 bottom	0.2342	0.2002	8.6383	3.3500
Intermediate zone top	0.2190	0.0880	3.7959	1.4723
Intermediate zone bottom	0.1250	0.1069	4.6151	1.7898
North soak zone top	0.0215	0.0172	0.7959	0.2888
North soak zone bottom	0.0245	0.0196	0.9067	0.3290
South soak zone top	0.0181	0.0172	0.7959	0.2888
South soak zone bottom	0.0215	0.0340	0.7959	0.5692

Temperature

Adjusting the fuel flow rates for the hydrogen case achieve the exact same temperature as the methane case was not very feasible. However, in this investigation as seen in Figure 40, we came close to similar average temperature across the reheat furnace with 18.3% reduction in fuel flow rates. The average temperature extracted from the simulation for the new hydrogen case was 1132K. This value is about 7K higher than the methane case and 51K lower than the initial hydrogen case.

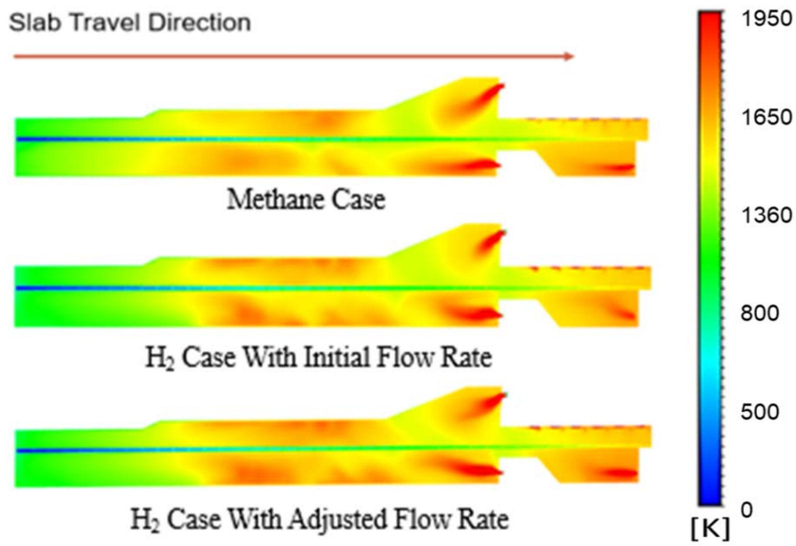

Figure 40. Temperature profile.

Heat flux

Decreasing the fuel flow rate by 18.3% to achieve a similar average furnace temperature as seen in the methane case significantly reduced the heat flux into the slab. The heat flux plot in Figure 41 shows heat flux into the slab. The average heat flux into the steel slab was 91kW/m^2, 92kW/m^2 and 99kW/m^2, for the methane, new hydrogen and initial hydrogen cases respectively. The difference in average heat flux of the new hydrogen case from the methane case was about 1% considering that the average temperature was 7K higher for the new hydrogen case. Heat flux values will be more similar if the average temperature was exactly the same.

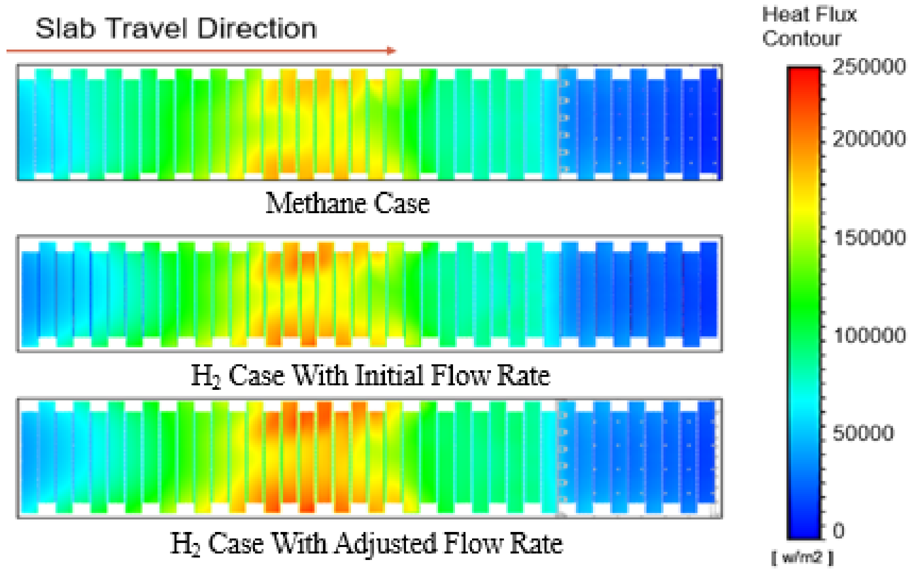

Figure 41. Heat flux profile.

5.5.2 Staged Combustion

In the study of hydrogen fuel utilization, researchers have come to discover that burning hydrogen produces higher NOx values than methane, a trend which was also observed in this work. Among several NOx reduction techniques for hydrogen combustion, there are just few that can be applicable to a reheating furnace of which staged combustion was selected to be studied in this work. This can be simply seen as a double staged combustion method. In this method, one can inject a fraction of the desired mass of air or fuel through a burner and another fraction through a lance near the burner. The purpose for this method, is to reduce the maximum ignition temperature thereby, lowering the thermal NOx value in the system. Staging the hydrogen will mean that the initial combustion through the burners will have excess air, making it a lean combustion and will in most cases result in higher ignition temperature hence, higher thermal NOx values. For this work, we staged the air as illustrated in the Figure 42 below to have an initial lower ignition temperature from a rich combustion. This type of combustion method promotes the generation of N_2 and the reduces NOx emission. Figure 42 below shows a portion of the modified furnace geometry accommodating an air lance between two burners. The air lance was only considered for the heating zones, because they are the zones with the largest mass flow rates.

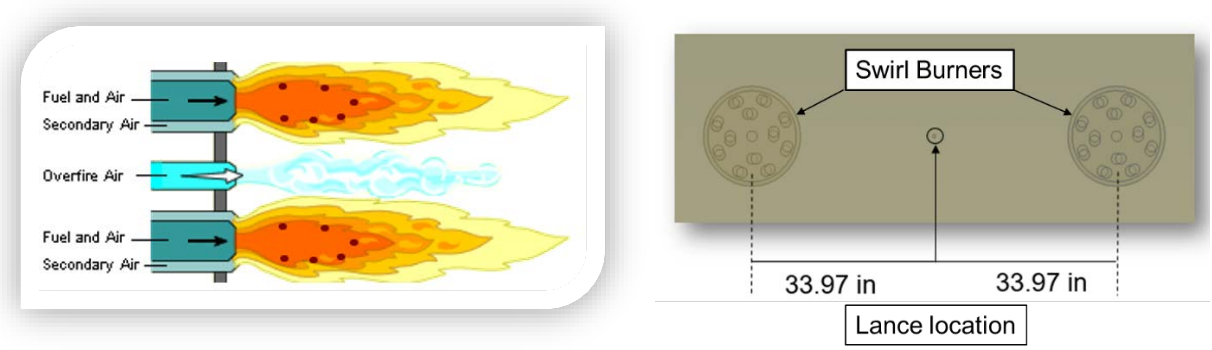

Figure 42. Staged combustion technique illustration and geometry modification.

To adequately simulate this technique, the air was made to enter the combustion domain at sonic velocity so as to allow the second stage of the combustion to occur at the center of the furnace and not at near to furnace walls. The Mach equation was used to solve for sonic velocity for air at 640K.

$$M = 1 = V/\sqrt{kRT} \tag{23}$$

k = 1.367 at 640K for air

R_{air} = 287.05 J/kg-K

$$V = \sqrt{1.367 * \frac{287.05J}{kg\ K} * (640K)} = 500 \text{ m/s}$$

Here the one dimensional isentropic flow formula for Mach number was used for simplicity. Where M is Mach number, V represents the velocity of the fluid, R is the individual gas constant and T, temperature of the fluid. Table 13 shows flow rates and lance diameters for the different cases and their zones.

Table 14. Boundary conditions for staged combustion cases.

	Case 2- 10% air through lance			**Case 3- 17.5% air through lance**				**Case 4- 25% air through lance**				
	HZ1 top	**HZ1 bot**	**HZ2 top**	**HZ2 bot**	**HZ1 top**	**HZ1 bot**	**HZ2 top**	**HZ2 bot**	**HZ1 top**	**HZ1 bot**	**HZ2 top**	**HZ2 bot**
Air in burner (kg/s)	4.25	5.67	7.26	7.76	3.90	5.20	6.65	7.11	3.54	4.73	6.05	6.47
Fuel in burner (kg/s)	0.13	0.17	0.22	0.23	0.13	0.17	0.22	0.23	0.13	0.17	0.22	0.23
Air in lance (kg/s)	0.47	0.63	0.81	0.86	0.83	1.10	1.41	1.51	1.18	1.58	2.02	2.16
Lance diameter (m)	0.01	0.01	0.02	0.02	0.02	0.02	0.02	0.02	0.02	0.02	0.03	0.03

Temperature

To investigate the temperature distribution in the furnace, a temperature contour was taken 0.03 inches above the slab. The contour plots in Figure 43 below shows that the staged combustion scenarios had a more symmetric temperature profile in contrast to the no staging case that showed patches of higher temperature heating zones.

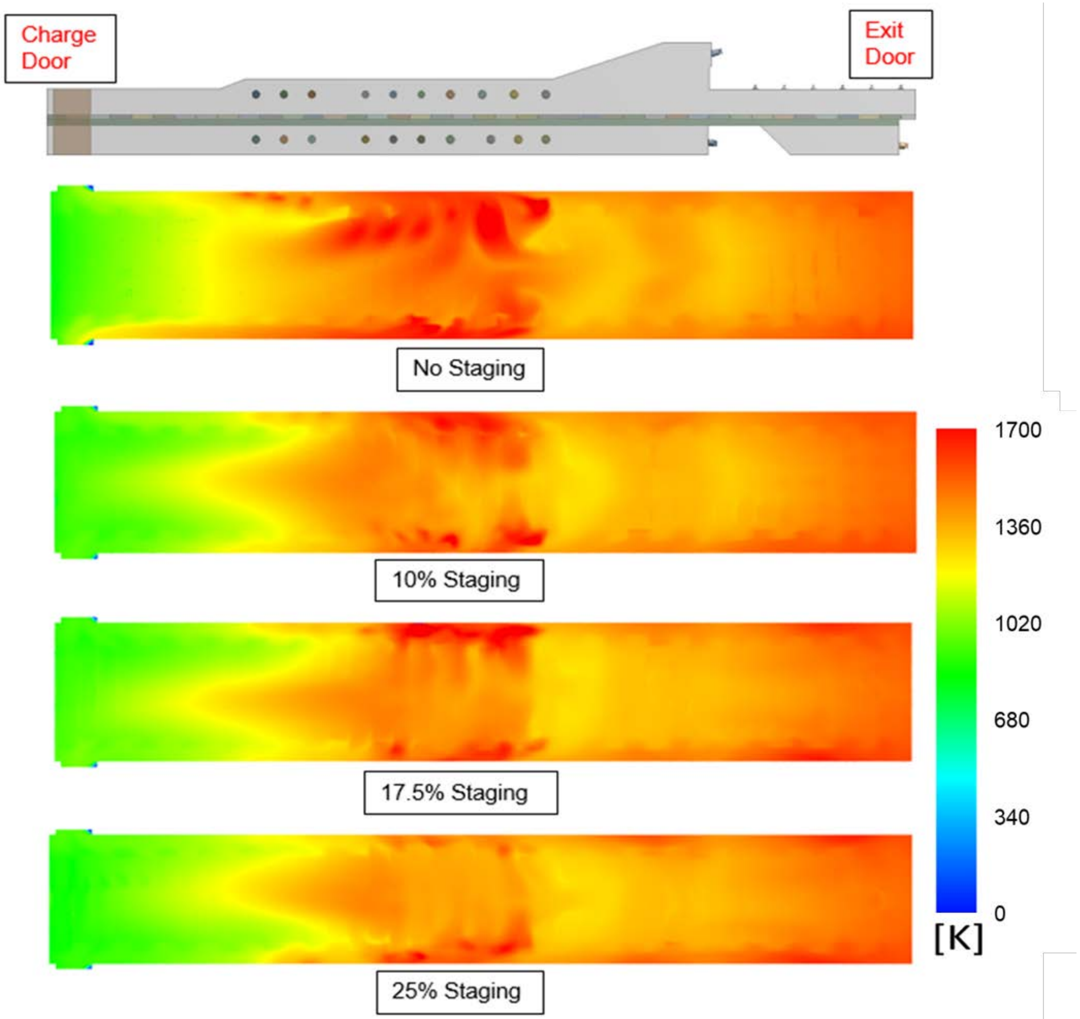

Figure 43. Temperature contour plots for staging cases.

Average temperature values were also seen to reduce by 2.5% for the 10% and 17.5% staging cases. It further dropped by 3.8% for the 25% staging case. From the plot in Figure 44 the lower temperatures can be clearly observed to occur mostly in the heating zones which were the zones with air lances and then in the preheating zone due to the flow of the lower temperature flue gas to the outlet. In the soak zone, no conspicuous temperature drop was recorded. The temperature drop observed in this investigation was as a result of lower initial ignition temperature of the rich combustion.

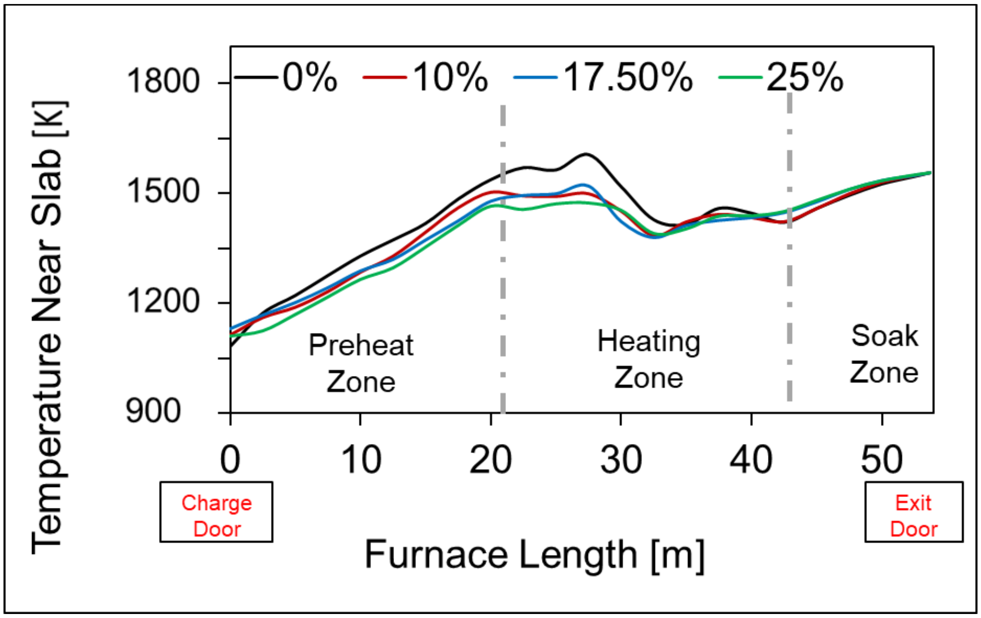

Figure 44. Temperature line plots across furnace for staging cases.

Heat flux

The effect of the lower temperature flue gases recorded in the staging scenarios was seen when the heat flux was investigated. 10%, 17.5% and 15% cases saw 8%, 10.5% and 15% reduction in average heat flux into the slab as can be seen from the line plots in Figure 45 This could result to a slightly lower productivity yield when compared to the no-staging hydrogen scenario as the slabs may need a longer dwell time to attain the desired temperature homogeneity. A careful study of the heat flux pattern also showed that staged combustion application will not adversely affect the thermal stress of the steel slab as the heat flux contour in Figure 46 shows a less steep gradient in the preheating zone regions.

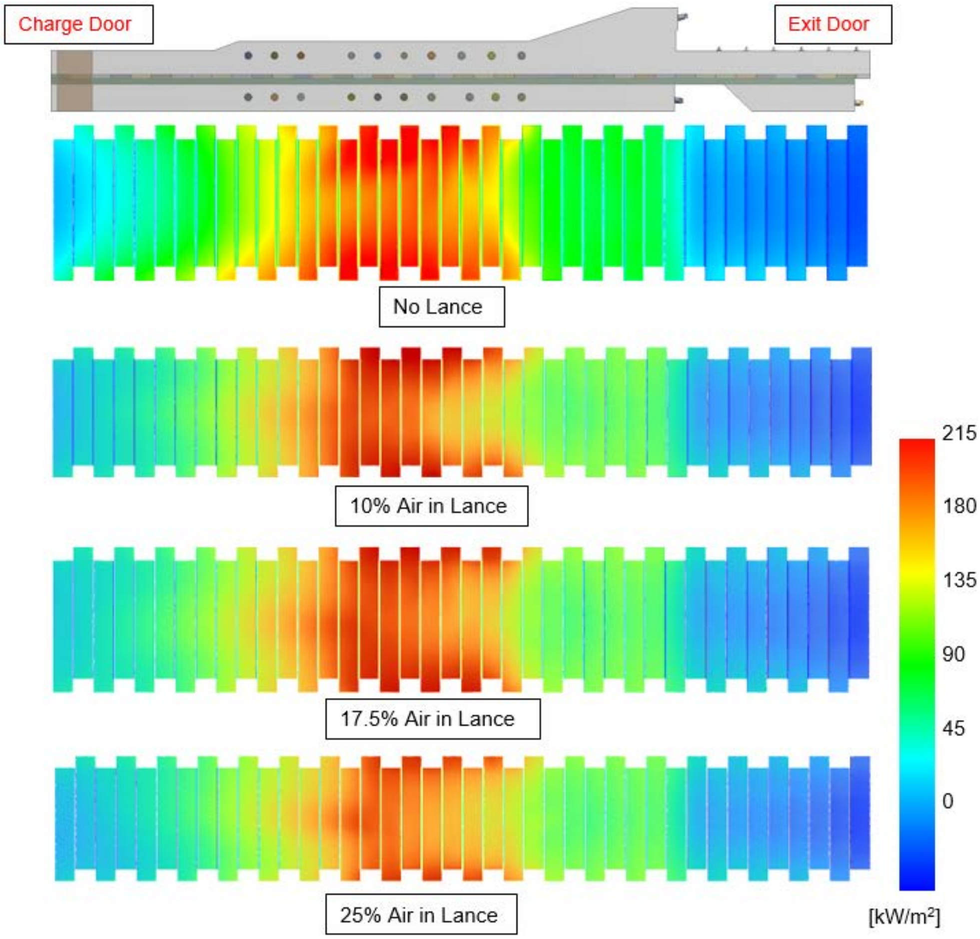

Figure 45. Heat flux contour plots for staging cases.

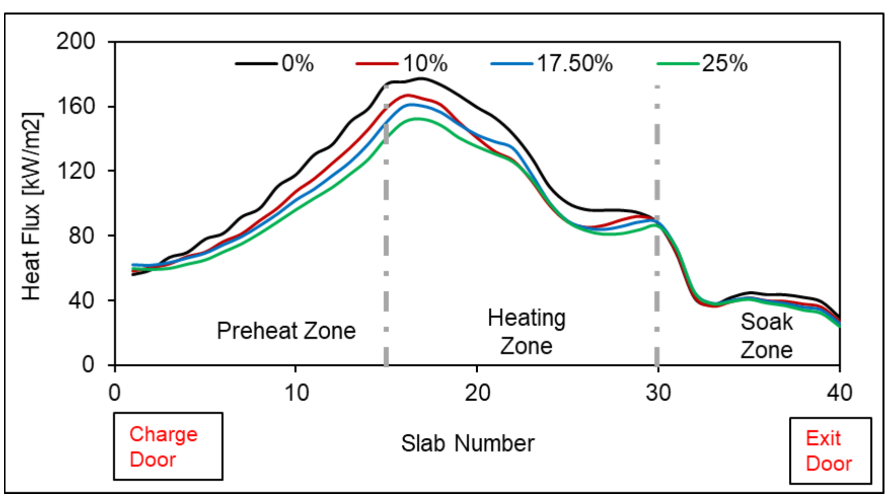

Figure 46. Heat flux line plots across furnace for staging cases.

Emissions

The NOx values were also seen to reduce with increase in the amount of air staged. However, after 17.5% staging the NOx value was seen to gradually increase at 25% air staged combustion. Another, major benefit of the staged combustion technique as seen from the results displayed in Table 14 is that aids in more complete combustion due to the double staged combustion technique. The more the staging the lesser the fuel seen at the flue gas outlet. This can help avoid fuel leakages and accumulation that might result in unwanted explosions since hydrogen is very light and largely unstable. The 17.5% staging case could be seen as the best case with respect to the 14.5% reduction in NOx values from the no-staging case.

Table 15. Flue gas concentrations and temperatures.

Case	H_2 (ppm)	O_2 (mol frac)	H_2O (mol frac)	NOx increase (%)	Avg furnace temp. (K)
Base Case (0%)	0.005	0.011	0.301	-	1478
Case 2 (10%)	1.8E-5	0.012	0.307	- 6.674	1446
Case 3 (17.5%)	9.67E-7	0.012	0.308	- 14.52	1440
Case 4 (25%)	3.1E-7	0.014	0.300	- 14.05	1424

Relative to methane

Even though the application of the staged combustion technique using hydrogen fuel may result in lower average temperature in the furnace than the no-staging combustion cases using hydrogen fuel, comparing it with a methane fired reheating furnace may prove otherwise, advantageous. Figure 47 below shows the average temperature across the furnace length from charge door to exit door. The 17.5% staging case has a 15K higher average temperature near the slab than the methane case.

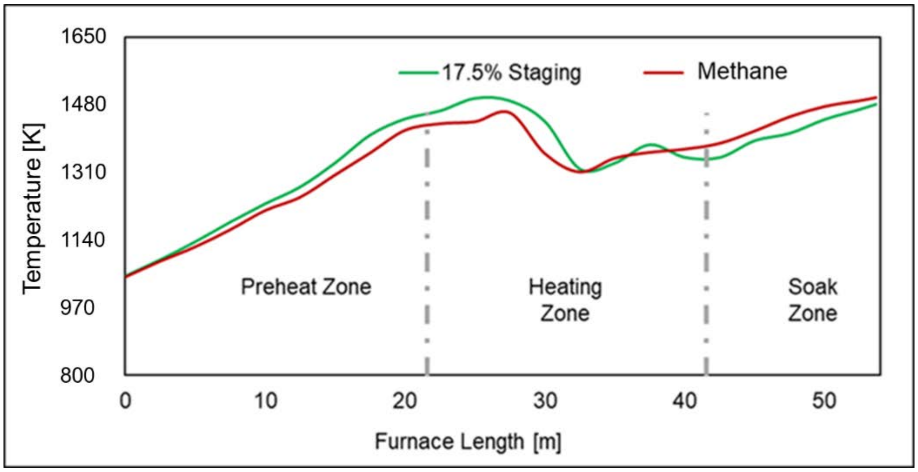

Figure 47. Line plots of 17.5% air staging vs. methane case.

Table 16. Heat flux and temperature values for17.5% air staging vs. methane case.

Case	Avg. temp near slab (K)	Avg. heat flux (kW/m^2)
Methane	1373	92
Case 3 (17.5%)	1381	90

The staging case showed superior temperature magnitude in the preheating zone and heating zone while the natural had higher temperatures in the soak zone region. However, the natural gas heat flux was about 2kW/m^2 higher than the staged combustion cases, which one could say is negligible considering numerical errors. In other words, the slab heating time for both conditions will not have a significant difference.

5.5.3 Regenerative burner application

The regenerative heating technique is a very energy efficient heating method where high temperature combustion products are intermittently stored in a thermal repository mechanism and in turn used to preheat the incoming combustion air. In applying this technique, burners from one side of the furnace is allow burn for a fixed amount of time and then turned off while burners on the other side of the furnace are burned as is illustrated in Figure 48 below. This intermittent burning technique continues until the slab is adequately heated.

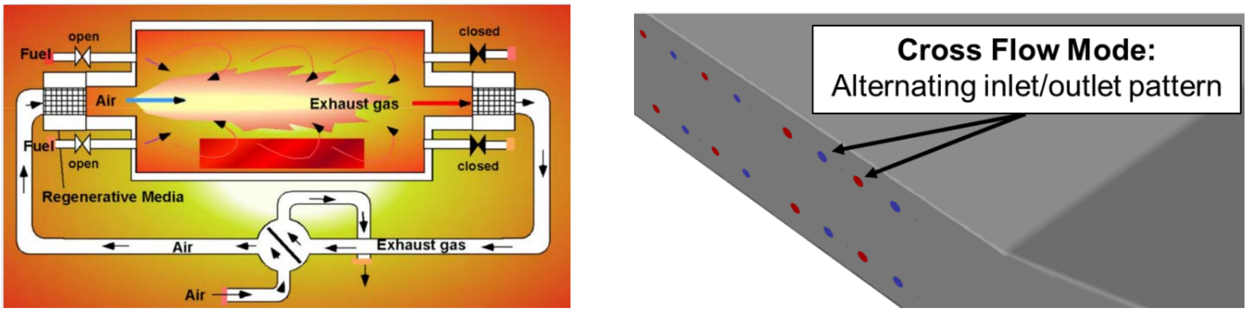

Figure 48. Regenerative burner illustration and geometry modifications.

Modifications and boundary conditions where applied to the existing furnace geometry to accommodate regenerative burner applications. The burners where represented as imprints on the surface of the furnace and using preheated air and fuel flow rates as boundary conditions. methane using the traditional reheating furnace with a heat input of 161MWh was compared with hydrogen using regenerative burners with a heat input of 120 MWh in a transient CFD simulation. The heat input values and flow rates matching them were provided by Fives Group and the regenerative burners were used in the heating and preheating zones only.

Temperature

After monitoring the slab temperature for 140 minutes in a transient simulation, the slab core average temperatures where investigated. A close look at the temperature line plot in the Figure 49 below shows that the core temperatures for both operating conditions had very similar temperature trend and values. The slabs exited the furnace at 1414K and 1422K for the hydrogen and methane cases respectively.

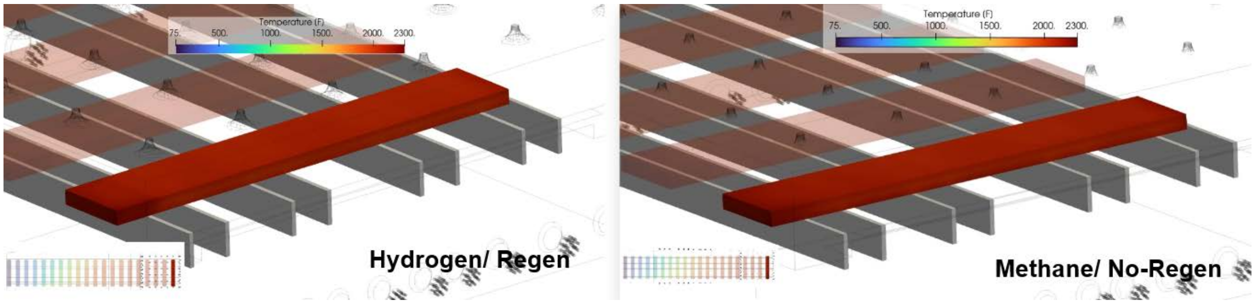

Figure 49. Slabs at exit for H_2 regenerative application and methane regular application.

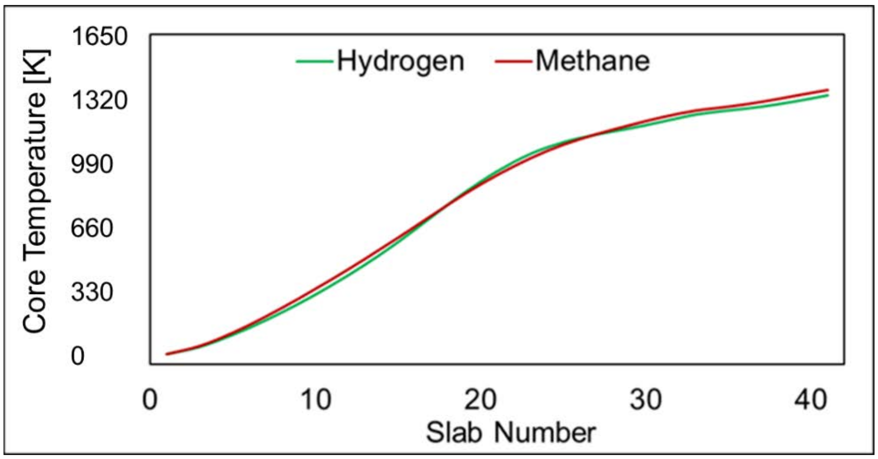

Figure 50. Temperature plots at slab core across furnace.

The slabs exited the furnace at 1414K and 1422K for the hydrogen and methane cases respectively as can be seen in Figure 50.

Heat flux

Heat flux contours taken from the simulation represented in Figure 51 showed a more symmetrical area of heat flux into the slabs for the regenerative burner case than the traditional burner case. The maximum heat flux for methane in the traditional burner case is 226 kW/m^2 and 276kW/m^2 for the hydrogen with regenerative burner case. However, the average heat flux considering all the zones was 92.3kW/m2 for both cases.

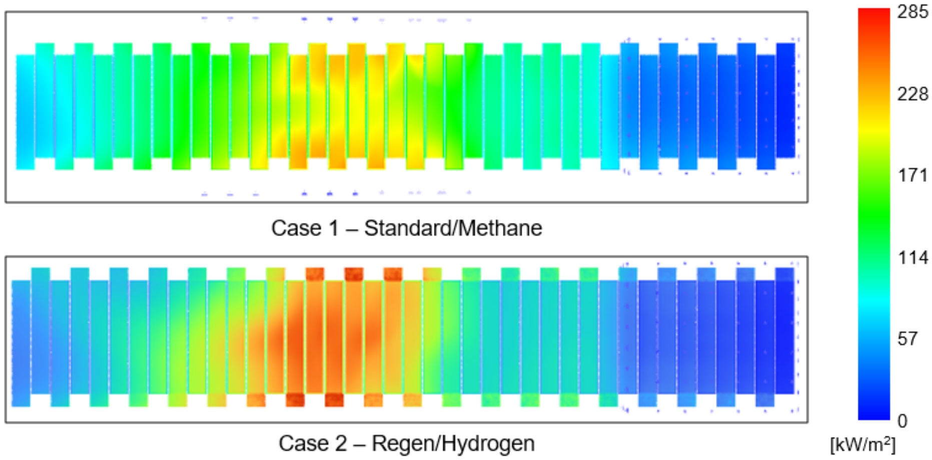

Figure 51. Heat flux contour plots.

From the above results one can see that with same average heat flux into the slabs can be achieved with 25% reduction in fuel related heat input into the reheating furnace by using regenerative burners.

6. CONCLUSIONS

Alternative fuels research to counteract carbon emissions is a global problem that has piqued the interest of various technical sectors, particularly the steel manufacturing sector. Research has revealed that hydrogen could be used to accomplish that goal since it’s a non-carbon-based energy source. However, it is important to investigate its combustion characteristics to see if it is a good match with respect to temperature profile, fluid flow and mode of heat transfer. The hydrogen model produced some intriguing insights that will help the steel sector

The validated furnace model has been used to investigate the application of hydrogen in the reheating furnace. The simulations show that the application of hydrogen as an operating fuel for reheat furnaces in the steel mill is not an impossible task. Application of hydrogen maintaining the same heat input as natural gas, gives a higher heat flux which can be translated to greater productivity from the furnace hereby having an economic advantage.

The hydrogen model gave positive results that will be beneficial to the steel industry. Results from the numerical simulation gave that not only did hydrogen as fuel increase the heat flux into the slab and eliminate carbon emission, it had no significant negative effect on the stresses in the slab. Adjusting the hydrogen fuel mass flow rate is a practical way of limiting scale development as it will result in lower combustion gas temperature.

Temperature change generates thermal stresses in the interior of the slab and surfaces. The thermal stress increases in the same range from zero minutes (charge door) to 14 minutes of residence time. After this range of time, the thermal stress starts to decrease. Higher stress can be noted at the skid positions, sides, slab core, and near to corners.

The numerical simulation results for all study instances utilizing the same furnace design, governing equations and chemical heat input produced the following results:

- Across the furnace length, hydrogen case achieved an average combustion temperature 3% higher than that of methane. This is due to the higher heating value of hydrogen, thereby resulting in higher flame temperatures.
- The flow of combustion gases on both methane and hydrogen cases revealed similar fluid flow patterns. However, fluid flow in natural gas was seen to be faster than hydrogen due to higher mass flow rate of the natural gas.
- The dominant heat transfer mode during the combustion of hydrogen in the reheating furnace was radiation. This made up 96.3% of the total heat flux into the slab during the reheating process. This result is favorable as it shows that the primary heat transfer mode in a reheat furnace was maintained with change of fuel.
- From the thermal stress analysis, lower thermal stresses were realized by hydrogen combustion due to the low temperature in the preheat zones that was as a result of the low velocity combustion gases of hydrogen in that zone. This slightly lower temperature resulted in a lower temperature gradient thereby slowing down the ramp up of thermal stress values in the slab. Overall, the maximum thermal stress values did not exceed the yield strength of the material.
- Higher scale thickness was realized when using hydrogen fuel, however, more of the wüstite which are easier to descale occupied a greater percentage. This shows tells descaling may not be difficult.
- The staged combustion technique can reduce NOx and temperature. However, the temperature reduction is not detrimental when compared to methane at the same fuel heat input.
- Energy efficiency of a reheating furnace can be improved by 25% by switching the regular burners to regenerative burners.
- Results from this study has shown that considering the factors focused on in this work, hydrogen combustion characteristics is similar to methane combustion and hence, a good replacement for methane in the reheating furnace operations.

To expand more in this research and further study the possibility of hydrogen replacing methane as an alternative for carbon elimination, further practices for optimization hydrogen application in the reheating furnace can be carefully explored. This will provide more detailed information about the ability to replace methane with hydrogen as a primary source of energy in the steel industry’s reheating furnaces.

7. FUTURE WORKS

In studying the staged combustion, the air lances where only put in the heating zones, further research can be done by investigating the reduction in NOx when the lances are installed in other zones of the reheating furnace. Further numerical analysis can be carried out using more detailed kinetic mechanisms for the hydrogen study and see how that can affect the parameters covered in this study. Investigation of hydrogen as fuel can explore several applications for optimization and application driven studies.

REFERENCES

[1] Flanagan, D. M., 2019, "Mineral Commodity Summaries, February 2019:Copper," U.S. Geol. Surv. Miner. Commod. Summ., **26**(1).

[2] Han, S. H., Chang, D., and Kim, C. Y., 2010, "A Numerical Analysis of Slab Heating Characteristics in a Walking Beam Type Reheating Furnace," Int. J. Heat Mass Transf., **53**(19–20), pp. 3855–3861.

[3] Liu, X., Worl, B., Tang, G., Silaen, A. K., Cox, J., Johnson, K., Bodnar, R., and Zhou, C. Q., 2019, "Numerical Simulation of Heat Transfer and Scale Formation in a Reheat Furnace," Steel Res. Int., **90**(4).

[4] Harish, J., and Dutta, P., 2005, "Heat Transfer Analysis of Pusher Type Reheat Furnace," Ironmak. Steelmak., **32**(2).

[5] Dubey, S. K., and Srinivasan, P., 2014, "Development of Three Dimensional Transient Numerical Heat Conduction Model with Growth of Oxide Scale for Steel Billet Reheat Simulation," Int. J. Therm. Sci., **84**, pp. 214–227.

[6] Price, L., Sinton, J., Worrell, E., Phylipsen, D., Xiulian, H., and Ji, L., 2002, *Energy Use and Carbon Dioxide Emissions from Steel Production in China*.

[7] Dincer, I., *Renewable Energy and Sustainable Development: A Crucial Review*.

[8] Severinsky, A. J., *Radiative Force on Ice, GHG Radiative Force on Plants, GHG Radiative Force in Air*.

[9] Cokain -Global Sales, K., Coordinator, A., and Cochran -Applications Engineer, M., *CO 2 Reduction Options for High Temperature Industrial Combustion*.

[10] Wu, L., Kobayashi, N., Li, Z., Huang, H., and Li, J., 2015, "Emission and Heat Transfer Characteristics of Methaneehydrogen Hybrid Fuel Laminar Diffusion Flame."

[11] Patel, V., and Shah, R., 2019, "Effect of Hydrogen Enrichment on Combustion Characteristics of Methane Swirling and Non-Swirling Inverse Diffusion Flame."

[12] Oh, J., Noh, D., and Ko, C., 2013, "The Effect of Hydrogen Addition on the Flame Behavior of a Non-Premixed Oxy-Methane Jet in a Lab-Scale Furnace."

[13] Hu, L., 2016, "A Simplified Practical Model for a Walking Beam Type Reheat Furnace with Specific Heat Transfer Characteristics," Int. J. Model. Optim., **2**(8).

[14] Venturino M., and Rubini P., 1995, “Coupled Fluid Flow and Heat Transfer Analysis of Steel Reheat Furnaces.”

[15] Emadi, A., Saboonchi, A., Taheri, M., and Hassanpour, S., 2014, “Heating Characteristics of Billet in a Walking Hearth Type Reheating Furnace,” Appl. Therm. Eng., **63**(1), pp. 396–405.

[16] Morgado, T., Coelho, P. J., and Talukdar, P., 2015, “Assessment of Uniform Temperature Assumption in Zoning on the Numerical Simulation of a Walking Beam Reheating Furnace,” Appl. Therm. Eng., **76**, pp. 496–508.

[17] Harish, J., and Dutta, P., 2005, “Heat Transfer Analysis of Pusher Type Reheat Furnace,” Ironmak. Steelmak., **32**(2), pp. 151–158.

[18] Jaklič, A., Vode, F., and Kolenko, T., 2007, “Online Simulation Model of the Slab-Reheating Process in a Pusher-Type Furnace,” Appl. Therm. Eng., **27**(5–6), pp. 1105–1114.

[19] Jang, J. H., Lee, D. E., Kim, M. Y., and Kim, H. G., 2010, “Investigation of the Slab Heating Characteristics in a Reheating Furnace with the Formation and Growth of Scale on the Slab Surface,” Int. J. Heat Mass Transf., **53**(19–20), pp. 4326–4332.

[20] Collin. R, 1968, “A Flexible Mathematical Model for the Simulation of Reheating Furnace Performance,” *Of Conference for Hot Working*.

[21] Krivandin .V. A., and Markov B. I., 1980, “Metallurgical Furnaces,” Mir Publ.

[22] Minaev A.N., Reshetnyak S.I., and Butenko I.G., 1983, “HEAT TRANSFER IN WALKING BEAM FURNACES,” Steel USSR, **13**(9), pp. 151–158.

[23] Tang, G., Wu, B., Bai, D., Wang, Y., Bodnar, R., and Zhou, C., 2018, “CFD Modeling and Validation of a Dynamic Slab Heating Process in an Industrial Walking Beam Reheating Furnace,” Appl. Therm. Eng., **132**, pp. 779–789.

[24] Kim, M. Y., 2007, “A Heat Transfer Model for the Analysis of Transient Heating of the Slab in a Direct-Fired Walking Beam Type Reheating Furnace,” Int. J. Heat Mass Transf., **50**(19–20), pp. 3740–3748.

[25] Singh, V. K., and Talukdar, P., 2013, “Comparisons of Different Heat Transfer Models of a Walking Beam Type Reheat Furnace,” Int. Commun. Heat Mass Transf., **47**, pp. 20–26.

[26] Prieler, R., Mayr, B., Demuth, M., Holleis, B., and Hochenauer, C., 2016, “Prediction of the Heating Characteristic of Billets in a Walking Hearth Type Reheating Furnace Using CFD,” Int. J. Heat Mass Transf., **92**, pp. 675–688.

[27] Lan, Y. J., Li, D. Z., Sha, X. C., and Li, Y. Y., 2004, “Prediction of Microstructure and Mechanical Properties of Hot Rolled Steel Strip: Part I - Description of Models,” Steel Res. Int., **75**(7).

[28] Hedayati, A., Najafizadeh, A., Kermanpur, A., and Forouzan, F., 2010, “The Effect of Cold Rolling Regime on Microstructure and Mechanical Properties of AISI 304L Stainless Steel,” J. Mater. Process. Technol., **210**(8).

[29] García, A. M., Colorado, A. F., Obando, J. E., Arrieta, C. E., and Amell, A. A., 2019, “Effect of the Burner Position on an Austenitizing Process in a Walking-Beam Type Reheating Furnace,” Appl. Therm. Eng., **153**.

[30] World Steel Association, 2020, “Steel Statistical Yearbook 2020 Concise Version. A Cross-Section of Steel Industry Statistics 2010-2019,” Worldsteel Assoc.

[31] Chen, S., 2009, “Modeling for Reheat Furnace Practices,” *Flat-Rolled Steel Processes: Advanced Technologies*.

[32] Barr, P. V., 1995, “The Development, Verification, and Application of a Steady-State Thermal Model for the Pusher-Type Reheat Furnace,” Metall. Mater. Trans. B, **26**(4).

[33] Yin, C., Rosendahl, L. A., and Kær, S. K., 2011, “Chemistry and Radiation in Oxy-Fuel Combustion: A Computational Fluid Dynamics Modeling Study,” Fuel, **90**(7), pp. 2519–2529.

[34] Abusayf, F., and Abuluwefa, H. T., 2016, “Thermal Efficiency in Steel Reheating Process,” Int. J. Eng. Inf. Technol., **3**(1), p. 58.

[35] Païdassi, J., 1958, “The Kinetics of the Air Oxidation of Iron in the Range 700-1250°C,” Acta Metall., **6**(3).

[36] Akiyama, T., Ohta, H., Takahashi, R., Waseda, Y., and Ichiroyagi, J., 1992, “Measurement and Modeling of Thermal Conductivity for Dense Iron Oxide and Porous Iron Ore Agglomerates in Stepwise Reduction,” ISIJ Int., **32**(7).

[37] Smeltzer, W. W., 1960, “The Kinetics of Wustite Scale Formation on Iron,” Acta Metall., **8**(6).

[38] Sachs, K., and Tuck, C. W., 1970, “Scale Growth during Re-heating Cycles,” Mater. Corros., **21**(11).

[39] Selenz, H. J., and Oeters, F., 1984, “CONTRIBUTION TO THE SCALING OF STEEL IN TECHNICAL FLUE GASES.,” Arch. fur das Eisenhuttenwes., **55**(5).

[40] Abuluwefa, H., 1996, "The Effect of Oxygen Concentration on the Oxidation of Low-Carbon Steel in the Temperature Range 1000 to 1250°C," Oxid. Met., **46**(5–6).

[41] Abuluwefa, H. T., Guthrie, R. I. L., and Ajersch, F., 1997, "Oxidation of Low Carbon Steel in Multicomponent Gases: Part I. Reaction Mechanisms during Isothermal Oxidation," Metall. Mater. Trans. A Phys. Metall. Mater. Sci., **28**(8).

[42] Mayr, B., Prieler, R., Demuth, M., Moderer, L., and Hochenauer, C., 2017, "CFD Analysis of a Pusher Type Reheating Furnace and the Billet Heating Characteristic," Appl. Therm. Eng., **115**.

[43] Himmel, L., Mehl, R. F., and Birchenall, C. E., 1953, "Self-Diffusion of Iron in Iron Oxides and The Wagner Theory of Oxidation," JOM, **5**(6).

[44] Deich, J., and Oeters, F., 1973, "Zur Verzunderung von Weichstahl in Stickstoff-Kohlendioxid-Gemischen Mit Geringen Sauerstoffzusätzen," Mater. Corros., **24**(5).